Turing Instability of a Closed Nutrient-Phytoplankton-Zooplankton Model with Nutrient Recycling

by

Xiangye Xu

A thesis
presented to the University of Waterloo
in fulfillment of the
thesis requirement for the degree of
Master of Mathematics
in
Applied Mathematics

Waterloo, Ontario, Canada, 2025

© Xiangye Xu 2025

Examining Committee Membership

The following served on the Examining Committee for this thesis. The decision of the Examining Committee is by majority vote.

Supervisor(s):	Francis Poulin Professor, Dept. of Applied Mathematics, University of Waterloo Sue Ann Campbell Professor, Dept. of Applied Mathematics, University of Waterloo
Internal Member:	Chris Bauch Professor, Dept. of Applied Mathematics, University of Waterloo
Internal Member:	Henry Shum Associate Professor, Dept. of Applied Mathematics University of Waterloo

Author's Declaration

I hereby declare that I am the sole author of this thesis. This is a true copy of the thesis, including any required final revisions, as accepted by my examiners.

I understand that my thesis may be made electronically available to the public.

Abstract

We investigate Turing instability in a closed Nutrient–Phytoplankton–Zooplankton (NPZ) ecosystem that incorporates delayed nutrient recycling, formulated as a reaction–diffusion system. Although spatial diffusion typically enhances system stability, our study focuses on how differing diffusion rates among species can destabilize steady states and lead to the emergence of spatial patterns. To explore this, we first perform a linear stability analysis to identify the conditions under which Turing instability arises. These theoretical predictions are then validated through numerical simulations. Our study progresses systematically: beginning with a two-species model, extending to a three-species system, and finally to a four-species NPZD model. This stepwise framework provides both conceptual insight and quantitative understanding of how diffusion influences instabilities, offering a comprehensive perspective on pattern formation in multi-species plankton ecosystems.

Acknowledgements

I would like to express my deepest gratitude to my supervisors, Professor Francis Poulin and Professor Sue Ann Campbell, for their continuous guidance, support, and encouragement throughout my research. Their insightful advice and patience have been invaluable in shaping both the direction and quality of this thesis. I am especially grateful to Francis for his instruction and assistance with numerical methods in Oceananigans, as well as for his thought-provoking questions that consistently deepened my understanding. I would also like to thank Sue Ann for her expertise and for guiding me with detailed, insightful feedback that greatly enhanced my problem-solving skills. Once again, I would like to express my deepest gratitude to my supervisors, Francis Poulin and Sue Ann Campbell, for guiding me through this remarkable journey as a master's student at the University of Waterloo.

I am also grateful to my colleagues and friends in the Fluids Lab, whose discussions, feedback, and companionship made my research experience both productive and enjoyable.

Finally, I would like to thank all the little people who made this thesis possible.

Dedication

I dedicate this thesis to my family and loved ones for their endless love, patience, and unwavering belief in me. Their support has made this achievement possible.

Table of Contents

Examining Committee ii

Author's Declaration iii

Abstract iv

Acknowledgements v

Dedication vi

List of Figures x

List of Tables xii

1 Introduction 1

1.1 Planktonic modeling 1

1.2 Turing instability 3

1.3 Contribution and outline 4

2 Planktonic Modeling 6

2.1 Ordinary Differential Equation Models 6

2.1.1 Nutrient-Phytoplankton (NP) Model 7

2.1.2 Nutrient-Phytoplankton-Zooplankton (NPZ) Model 7

2.1.3 Nutrient-Phytoplankton-Zooplankton-Detritus (NPZD) Model . . 8

2.2 Spatially Dependent Models . . . 9
2.2.1 NP model . . . 9
2.2.2 NPZ model . . . 10
2.2.3 NPZD model . . . 10
2.2.4 Conservation laws . . . 11

3 Linear Stability Analysis **13**
3.1 NP Model . . . 14
3.1.1 Equilibrium . . . 15
3.1.2 Stability without Diffusion . . . 15
3.1.3 Diffusion induced Instability . . . 16
3.2 NPZ Model . . . 18
3.2.1 Equilibrium . . . 18
3.2.2 Stability without Diffusion . . . 19
3.2.3 Diffusion induced Instability . . . 20
3.3 NPZD Model . . . 22
3.3.1 Equilibrium . . . 23
3.3.2 Stability without Diffusion . . . 24
3.3.3 Diffusion induced Instability . . . 26

4 Results **29**
4.1 Numerical Methods . . . 29
4.1.1 Parameter . . . 30
4.2 NP Model . . . 31
4.2.1 Stability Without Diffusion . . . 31
4.2.2 Diffusion Induced Instability . . . 32
4.2.3 Nonlinear simulations . . . 34
4.3 NPZ Model . . . 36
4.3.1 Stability Without Diffusion . . . 37

4.3.2 Diffusion Induced Instability 38
4.3.3 Nonlinear Simulations 39
4.4 NPZD Model 42
4.4.1 Stability Without Diffusion 43
4.4.2 Diffusion Induced Instability 43
4.4.3 Nonlinear simulations 45

5 Conclusion **51**

References **53**

APPENDICES **56**

A Supplementary Figures **57**

List of Figures

4.1 Dependence of linear growth rate of PDE model (2.3) on total biomass N_T and phytoplankton diffusion rate d_2 for modes k as shown. Other parameters values are given in Table 4.1 32

4.2 Dependence of linear growth rate of PDE model (2.3) on wave number k with $m = 0.5$. All other parameter values can be found in Table 4.1. 33

4.3 Dependence of linear growth rate of PDE model (2.3) on wave number k and phytoplankton mortality power m. All other parameter values can be found in Table 4.1. 34

4.4 Evolution of NP model after initial perturbation with $k = 4$ mode 35

4.5 Evolution of NP model with random initial perturbation 36

4.6 Dependence of linear growth rate of the ODE system (3.12) on the total biomass, N_T. Other parameter values are given in Table 4.2. 37

4.7 Dependence of linear growth rate of PDE model (2.6) on total biomass N_T and nutrient diffusion rate d_1 for modes k as shown. Other parameters values are given in Table 4.2. 38

4.8 Dependence of linear growth rate of PDE model (2.6) on wave number k with $m = 0.5$. Other parameters values are given in Table 4.2. 39

4.9 Dependence of linear growth rate of PDE model (2.6) on wave number k and phytoplankton mortaility power m. Other parameters values are given in Table 4.2. 40

4.10 Evolution of NPZ model after initial perturbation with $k = 2$ mode. . . . 41

4.11 Evolution of NPZ model with random initial perturbation 42

4.12 Longer Time Evolution of NPZ model after random initial perturbation . 43

4.13 Dependence of linear growth rate of the ODE system (2.2) on the total biomass, N_T. Other parameter values are given in Table 4.3. 44

4.14 Dependence of linear growth rate of PDE model (2.9) on total biomass N_T and nutrient diffusion rate d_1 for modes k as shown. Other parameters values are given in Table 4.3 45

4.15 Dependence of linear growth rate of PDE model (2.9) on wave number k and phytoplankton mortality power m. Other parameters are given in Table 4.3. 46

4.16 Dependence of linear growth rate of PDE model (2.9) on wave number k with $m = 0.5$. Other parameter are given in Table 4.3. 47

4.17 Evolution of NPZD model after initial perturbation with $k = 3$ mode . . . 48

4.18 Evolution of NPZD model with random initial perturbation 49

4.19 Longer Time Evolution of NPZD model after random initial perturbation 50

A.1 Evolution of NP model after initial perturbation with $k = 4$ and $d_2 = 0.004$. Other parameter values are given in Table 4.1. 57

A.2 Linear fit of logarithm growth of simulation in Figure 4.4 58

A.3 Power spectrum from Fourier decomposition of simulation in Figure 4.4 . 58

A.4 Evolution of NP model after random initial perturbation with $d_2 = 1$. Other parameter values are given in Table 4.1. 59

A.5 Power spectrum from Fourier decomposition of simulation in Figure 4.5 . 59

A.6 Evolution of NPZ model after initial perturbation with $k = 2$ and $d_1 = 0.1$. Other parameter values are given in Table 4.2. 60

A.7 Linear fit of logarithm growth of simulation in Figure 4.10 60

A.8 Power spectrum from Fourier decomposition of simulation in Figure 4.10 61

A.9 Evolution of NP model after random initial perturbation with $d_1 = 0.1$. Other parameter values are given in Table 4.2. 61

A.10 Power spectrum from Fourier decomposition of simulation in Figure 4.11 62

A.11 Linear fit of logarithm growth of simulation in Figure 4.17 62

A.12 Evolution of NPZD model after random initial perturbation with $d_1 = 0.05$. Other parameter values are given in Table 4.3. 63

A.13 Power spectrum from Fourier decomposition of simulation in Figure 4.18 64

A.14 Evolution of NPZD model after initial perturbation with $k = 3$ and $d_1 = 0.1$. Other parameter values are given in Table 4.3. 65

List of Tables

3.1 Types of equilibrium states in the NP model. 15
3.2 Types of equilibrium states in the NPZ model. 19
3.3 Types of equilibrium states in the $NPZD$ model. 24

4.1 NP Model Parameter 30
4.2 NPZ Model Parameter 30
4.3 NPZD Model Parameter 31

Chapter 1

Introduction

Planktonic ecosystems form the foundation of marine food webs and play a vital role in the regulation of the global carbon cycle. Due to their wide distribution and strong reproductive capacity, plankton serve as a primary food source for larger organisms, including zooplankton, small fish and other marine species. Consequently, understanding the dynamics of plankton populations is essential to elucidate broader ecological and bio-geochemical processes. To capture the spatial and temporal behavior of planktonic populations more realistically, diffusion terms are introduced into mathematical models. These diffusion components represent the spatial dispersal and mixing of plankton concentrations, preventing unrealistic aggregation of populations at single spatial points. In addition, the inclusion of diffusion can lead to the emergence of spatial structures under certain conditions—a phenomenon known as the Turing instability or the formation of Turing patterns. Such patterns are widely observed in nature, for example, in the structures of the bull's-eye colony of Proteus mirabilis [1].

The objective of this thesis is to investigate Turing instability within a planktonic ecosystem model to understand how diffusion can drive the emergence and evolution of spatial patterns in marine plankton populations.

1.1 Planktonic modeling

Given their crucial role in marine ecosystems, planktonic systems have been extensively investigated through mathematical modeling to better understand their dynamics. The review paper by Gentleman [10] provides a comprehensive overview of the chronological development of planktonic ecosystem models. Early modeling efforts focused on simple representations, such as the two-compartment prey–predator systems describing the interactions between phytoplankton and zooplankton. As research progressed,

more complex structures were proposed, including three-compartment models that incorporate nutrients, phytoplankton, and zooplankton (commonly referred to as NPZ models). From the 1980s to the 1990s, advances in computational power and conceptual understanding allowed such models to evolve into powerful tools for hypothesis testing and ecological prediction.

The coupling between physical and biological processes plays a critical role in shaping plankton dynamics and marine ecosystem structure. Physical mechanisms such as advection, turbulent mixing, and stratification regulate nutrient availability and light penetration, thereby influencing biological productivity and species distributions. Franks et al. [9, 8] unified physical and biological processes in NPZ-type models, illustrating how hydrodynamic variability modulates plankton growth and ecosystem stability. Several studies have explicitly modeled or documented this coupling between physical processes and biological dynamics. A coupled hydrodynamic–biological framework developed in [3] illustrates how flow and mixing govern algal growth and nutrient cycling. High-resolution observations presented in [17] reveal that mesoscale and sub-mesoscale features structure phytoplankton communities. Additional modeling efforts, such as those in [26], they use an advection–reaction–diffusion PDE model for phytoplankton, explicitly coupling large-scale flow (advection) and turbulent diffusion with reaction kinetics. A broader synthesis is provided by [22], which emphasizes that multi-scale biophysical coupling underlies many emergent ecological patterns.

In modeling planktonic dynamics, researchers place particular emphasis on nutrient recycling. Nutrient dynamics is typically characterized by inflow and outflow processes. Inflows generally arise from the mortality of phytoplankton and zooplankton, whereas outflows occur through interactions between nutrients, phytoplankton and zooplankton, such as nutrient uptake by phytoplankton or grazing by zooplankton. However, the transformation of dead planktonic biomass back into nutrients does not occur instantaneously. Nutrient recycling describes such transformation process which is the flow of biomass into the nutrient compartment from losses in the other compartments.

Furthermore, it is often reasonable to assume that the exchange of biomass between system boundaries is negligible. In other words, no substantial inflow of external species or outflow of internal biomass is considered. Models built under this assumption are commonly referred to as closed systems. In such systems, total biomass is conserved and variations in concentrations result solely from internal transfers among nutrients, phytoplankton, and zooplankton. As shown in [13], this closed-system framework can be used to study planktonic dynamics. This assumption is generally appropriate for modeling large-scale or relatively self-contained ecosystems, such as lakes or open-ocean regions. In contrast, open- or small-scale systems, such as laboratory chemostats or restricted water columns, experience significant inflows and outflows.

In these cases, biomass may be lost through physical removal (washout) or gained via external input, and such processes must be explicitly incorporated into the model formulation.

The importance of explicitly incorporating nutrient recycling into planktonic models has been emphasized in previous work [2], distinguishing them from chemostat-type formulations. Based on this perspective, [11] demonstrated that delayed nutrient recycling in chemostat-type plankton models can enhance the global stability of the system.

More recently, [12] showed that introducing a specific form of delay in nutrient recycling within a closed NPZ model is mathematically equivalent to extending the framework to an NPZD model by explicitly including detritus as a fourth compartment. It was also shown in [12] that introducing a delay in nutrient recycling in a closed NPZ system tends to raise the biomass threshold required for coexistence equilibria to exist and remain stable, thereby stabilizing these equilibria against oscillations for small to moderate delays. In this extended formulation, detritus represents the dead biomass of phytoplankton and zooplankton that slowly decomposes into dissolved nutrients, thus completing the nutrient cycle and enhancing the ecological realism of the model.

Building on these foundational contributions, our study incorporates delayed nutrient recycling within a closed NPZD ecosystem framework to further explore its effects on the spatiotemporal dynamics of planktonic systems.

1.2 Turing instability

In systems involving the spatial assembly of particles such as bacteria, chemicals, or biological species, diffusion plays a crucial role in describing how these entities spread over space. Under certain conditions, diffusion-driven instability, also known as Turing instability, may occur. This phenomenon arises when a spatially uniform steady state, stable in the absence of diffusion, becomes unstable once diffusion is introduced, leading to the emergence of spatially heterogeneous patterns.

Intuitively, diffusion is typically associated with stabilization, as it tends to smooth out spatial gradients over time. For example, in the classical heat diffusion equation, regions with stronger spatial gradients exhibit larger time derivatives, causing heat to flow from areas of high concentration to low concentration, and thereby promoting uniformity. Reaction–diffusion systems describe the combined effects of species reactions and spatial diffusion on the dynamics of a system. Interestingly, in such systems, diffusion can paradoxically induce instability, giving rise to organized spatial structures.

Accurate representation of diffusion processes is crucial in planktonic ecosystem models, as it governs nutrient transport and the spatial distribution of biological pop-

ulations. Empirical estimates of vertical eddy diffusivity have been obtained from observed phytoplankton and nutrient profiles, allowing parameterization of vertical mixing in models [20]. These studies highlight how field and experimental observations can constrain the diffusion coefficients of nutrients, phytoplankton, and zooplankton, ensuring biologically consistent model parameterizations.

Tao et al. [25] analyzed a diffusive nutrient-phytoplankton-zooplankton (NPZ) model that incorporates both temporal and spatial delays assuming the same diffusion constant for all species, and showed that diffusion can have a stabilizing effect under specific conditions. Murray et al. [18] provided a general theoretical framework for Turing instability in two-compartment reaction–diffusion systems, deriving general conditions under which interactions between species lead to instability. More recently, [15] investigated Turing instability in a two-compartment planktonic model, further extending these theoretical insights to marine ecosystems. In addition, [7] studied reaction–diffusion–advection equations for a single planktonic species by examining the asymptotic profiles of positive steady states under small and large diffusion limits.

Recent work has explored Turing-type mechanisms in more realistic open or partially coupled systems, where boundary fluxes and external forcing play a crucial role in pattern selection [14]. Extensions to reaction–diffusion–ODE models further reveal that coupling between diffusive and non-diffusive species can induce Turing patterns [16]. Moreover, studies in predator–prey systems with nonlinear cross-diffusion and Allee effects demonstrate that Turing instability can emerge under biologically plausible parameter regimes [23], while investigations in spatially heterogeneous domains show that environmental variability strongly influences pattern onset and morphology [28]. Moreover, Villar-Sepúlveda et al. [29] established the general conditions under which an n-component reaction-diffusion system can exhibit Turing, and [30] extended this work by providing a constructive framework for designing n-component reaction–cross-diffusion systems that produce such instabilities through appropriate choices of diffusion tensors and linearized reaction kinetics.

1.3 Contribution and outline

Our study progresses from two- and three-compartment to four-compartment reaction-diffusion models. Following [12] and [25], we adopt the same biological reaction terms to ensure consistency with established formulations. It is important to note that our modeling framework differs from these studies in the spatial component: [12] omits diffusion, and [25] includes diffusion but restricts all species to share the same diffusion constant. In contrast, our model allows different diffusion coefficients for all species.

We assume that the biological system is both conservative and diffusion-driven. Conservation and diffusion-driven are two strong conditions that can potentially stabilize the system. We demonstrate that variations in the relative scales of diffusion coefficients can give rise to Turing instability.

We systematically analyze Turing instability across models of increasing complexity: starting with a two-species nutrient-phytoplankton (NP) system, then extending to a three-species nutrient-phytoplankton-zooplankton (NPZ) model, and finally considering a four-species nutrient-phytoplankton-zooplankton-detritus (NPZD) formulation. For each case, we compare the analytical growth rates of perturbations derived in the model chapter with the approximate growth observed in numerical simulations. This step-by-step approach not only allows for verification of our analytical predictions but also builds intuition about how additional biological compartments influence the emergence and evolution of spatial patterns.

Chapter 2

Planktonic Modeling

2.1 Ordinary Differential Equation Models

Building on previous NPZ modeling studies [9, 8, 12], we consider a closed nutrient–phytoplankton model to investigate the onset of Turing instability. We then extend this analysis to a nutrient–phytoplankton–zooplankton system that incorporates nutrient recycling. Building from a simple model to a complicated model can give a better understanding and intuition of Turing instability. For simplicity, we only consider the variation of the populations in one space dimension, which corresponds to the depth of the water column; however, future studies can easily investigate what arises in higher dimensions.

In our planktonic models, each biological species is described by growth and loss terms. The growth of a species arises from nutrient uptake or, in the case of zooplankton, grazing on phytoplankton. Dissolved nutrients increase through the decomposition of biomass from other species. Each species experiences loss due to natural mortality or consumption by other species. Although individual growth and loss terms are not conservative by themselves, the overall system is biomass-conservative because each loss term in one equation appears as a corresponding growth term in another. Since we are more interested in large scale or self-contained ecosystem modeling, conservation of the total biomass can be derived with no-flux conditions across the boundary. Assuming the inflow and outflow of biomass at the boundaries is negligible leads to the conservation of total biomass. This is a very important assumption for our research.

2.1.1 Nutrient-Phytoplankton (NP) Model

A two-compartment model is used to construct a closed Nutrient–Phytoplankton (NP) system, where $N(t)$ and $P(t)$ denote the concentrations of nutrients and phytoplankton, respectively, as functions of time t.

In this section, we consider only the reaction terms that govern the dynamics of nutrient and phytoplankton. To ensure the conservation of total biomass, the reaction term for nutrients is defined as the negative of that for phytoplankton. The first term represents the uptake of nutrients by phytoplankton, corresponding to nutrient loss and phytoplankton growth. This term is modeled as the product of the phytoplankton concentration $P(t)$ and a general functional response $f(N(t))$ that describes nutrient dependence and the format of f is discussed in equation (2.1). The second term accounts for phytoplankton mortality, through which dead phytoplankton are converted back into dissolved nutrients, representing nutrient recycling. This term is assumed to be proportional to the m^{th} power of the phytoplankton concentration.

The model can thus be expressed by the following system of equations:

$$\begin{aligned}\frac{dN}{dt} &= -\nu P(t) f(N(t)) + \lambda P^m(t) \\ \frac{dP}{dt} &= \nu P(t) f(N(t)) - \lambda P^m(t)\end{aligned}$$

The rational power m of the death rate of phytoplankton plays a vital role in determining the possibility of the Turing Instability in the two compartmental model. Many authors take $m = 1$ [12, 25], but we will explore the effect of different values of m on the system dynamics in section 4.2.2.

2.1.2 Nutrient-Phytoplankton-Zooplankton (NPZ) Model

By introducing an additional species, zooplankton, as the predator of phytoplankton, we obtain a more comprehensive closed Nutrient–Phytoplankton–Zooplankton (NPZ) model, where $Z(t)$ denotes the concentration of zooplankton at time t:

$$\begin{aligned}\frac{dN}{dt} &= -\nu P(t) f(N(t)) + \lambda P^m(t) + \delta Z(t) \\ \frac{dP}{dt} &= \nu P f(N(t)) - g Z(t) h(P(t)) - \lambda P^m(t) \\ \frac{dZ}{dt} &= g Z(t) h(P(t)) - \delta Z(t)\end{aligned}$$

In this formulation, two new terms are introduced relative to the NP model: the growth rate and death rate of zooplankton. The nutrient loss term remains unchanged, whereas the nutrient growth term now includes nutrient recycling associated with the natural mortality of both phytoplankton and zooplankton. The natural death rate of zooplankton is modeled as being proportional to its current concentration. The zooplankton growth term corresponds to the phytoplankton death term, as zooplankton graze on phytoplankton at a rate that is linearly proportional to the product of their own concentration and a general function $h(P(t))$ of the phytoplankton concentration. In this NPZ model, the mortality of phytoplankton and zooplankton is assumed to be instantaneously converted into nutrients, such that the nutrient growth rate equals the sum of their respective mortality rates. In other words, the NPZ model represents a closed dynamical system without any time delay in nutrient recycling.

It is biologically reasonable to assume that the functions f and h are positive, increasing, zero at zero, and bounded above [8, 10, 12]. There are many functions that satisfy these conditions, here we focus on the Michaelis-Menten, also called Holling Type II [10],

$$f(u) = \frac{u}{u+k}, \qquad h(u) = \frac{u}{u+K}. \tag{2.1}$$

As in [12, 21], we assume $k = K = 1$. The study by [10] emphasizes that the choice of functional form can significantly influence plankton dynamics, such as the strength of top–down control and the emergence of oscillatory or stable behaviors.

2.1.3 Nutrient-Phytoplankton-Zooplankton-Detritus (NPZD) Model

The NPZ model discussed in the previous section does not account for the delay effect in nutrient recycling. Motivated by the work of Franks et al. [8], Kloosterman et al. [12] showed that a Nutrient-Phytoplankton-Zooplankton-Detritus (NPZD) model can be equivalent to an NPZ model with delayed nutrient recycling:

$$\begin{aligned}
\frac{dN}{dt} &= -\nu P(t) f(N(t)) + \alpha D(t) \\
\frac{dP}{dt} &= \nu P(t) f(N(t)) - \lambda P^m(t) - g Z(t) h(P(t)) \\
\frac{dZ}{dt} &= g Z(t) h(P(t)) - \delta Z(t) \\
\frac{dD}{dt} &= \lambda P^m(t) + \delta Z(t) - \alpha D(t).
\end{aligned} \tag{2.2}$$

In the NPZD model, the planktonic biomass is first transferred to the detritus, such that the growth rate of the detritus is equal to the combined mortality rates of phy-

toplankton and zooplankton. The detritus is subsequently converted into dissolved nutrients at a specified rate. Consequently, the NPZD model introduces an additional step in the nutrient recycling process, while the death and growth terms for the other components remain identical to those of the NPZ model.

2.2 Spatially Dependent Models

In the previous section, we primarily discussed the reaction component of the model. In this section, we extend the formulation to a model with spatial variations, which yields a system of PDEs, by adding diffusion to each biological species, thus forming a reaction–diffusion system. We allow nutrient, phytoplankton, zooplankton, and detritus to have different diffusion coefficients, denoted by d_1, d_2, d_3, d_4, respectively. This differs from previous studies employing similar models, such as [25], where all diffusion coefficients were assumed to be equal. In that case, it is shown that Turing instabilities cannot occur.

2.2.1 NP model

Keeping the same reaction parts of the spatially uniform models, we introduce the spatial diffusion for nutrient and phytoplankton with different diffusion coefficient d_1 and d_2. We obtain the following spatially dependent NP model:

$$\begin{aligned} \frac{\partial N(x,t)}{\partial t} &= d_1 \frac{\partial^2 N}{\partial x^2} - \nu P f(N) + \lambda P^m \\ \frac{\partial P(x,t)}{\partial t} &= d_2 \frac{\partial^2 P}{\partial x^2} + \nu P f(N) - \lambda P^m \end{aligned} \tag{2.3}$$

We impose the Neumann boundary condition for each species, which ensures that no biomass is lost through the boundary:

$$\frac{\partial}{\partial x}[N,P](x,t) = [0,0] \quad \text{for} \quad x = 0, 2\pi, \quad \text{and} \quad t \geq 0. \tag{2.4}$$

Our initial conditions are as follows.

$$[N,P,](x,0) = [N_0, P_0](x), \quad \text{for } x \in [0, 2\pi]. \tag{2.5}$$

We will explore some specific forms for the functions $N_0(x), P_0(x)$ in chapter 4.

2.2.2 NPZ model

Building on the previous NPZ spatially uniform model, the spatial diffusions for nutrient, phytoplankton and zooplankton with different diffusion coefficient d_1, d_2 and d_3 are imposed. We obtain the following spatially dependent NPZ model:

$$\begin{aligned}
\frac{\partial N(x,t)}{\partial t} &= d_1 \frac{\partial^2 N}{\partial x^2} - \nu P f(N) + \delta Z + \lambda P^m \\
\frac{\partial P(x,t)}{\partial t} &= d_2 \frac{\partial^2 P}{\partial x^2} + \nu P f(N) - \lambda P^m - gZh(P) \\
\frac{\partial Z(x,t)}{\partial t} &= d_3 \frac{\partial^2 Z}{\partial x^2} + gZh(P) - \delta Z
\end{aligned} \tag{2.6}$$

The following Neumann boundary condition is used for each species for NPZ model:

$$\frac{\partial}{\partial t}[N,P,Z](x,t) = [0,0,0] \quad \text{for} \quad x = 0, 2\pi, \quad \text{and} \quad t \geq 0. \tag{2.7}$$

Our initial conditions are as follows,

$$[N,P,Z](x,0) = [N_0, P_0, Z_0](x), \quad \text{for } x \in [0, 2\pi]. \tag{2.8}$$

We will explore some specific forms for the functions $N_0(x), P_0(x), Z_0(x)$ in chapter 4.

2.2.3 NPZD model

Building on the previous NPZD spatially uniform model, the spatial diffusions for nutrient, phytoplankton, zooplankton and detritus with different diffusion coefficient d_1, d_2, d_3 and d_4 are imposed. We obtain the following spatially dependent NPZD model:

$$\begin{aligned}
\frac{\partial N(x,t)}{\partial t} &= d_1 \frac{\partial^2 N}{\partial x^2} - \nu P f(N) + \alpha D \\
\frac{\partial P(x,t)}{\partial t} &= d_2 \frac{\partial^2 P}{\partial x^2} + \nu P f(N) - \lambda P^m - gZh(P) \\
\frac{\partial Z(x,t)}{\partial t} &= d_3 \frac{\partial^2 Z}{\partial x^2} + gZh(P) - \delta Z \\
\frac{\partial D(x,t)}{\partial t} &= d_4 \frac{\partial^2 D}{\partial x^2} + \lambda P^m + \delta Z - \alpha D
\end{aligned} \tag{2.9}$$

We use the Neumann boundary condition for $NPZD$ model as well:

$$\frac{\partial}{\partial t}[N,P,Z,D](x,t) = [0,0,0,0] \quad \text{for} \quad x = 0, 2\pi, \quad \text{and} \quad t \geq 0. \tag{2.10}$$

Our initial conditions are as follows,

$$[N,P,Z,D](x,0) = [N_0, P_0, Z_0, D_0](x), \quad \text{for } x \in [0, 2\pi]. \tag{2.11}$$

We will explore some specific forms for the functions $N_0(x), P_0(x)$ in chapter 4.

2.2.4 Conservation laws

We introduce the conservation law of $NPZD$ model, the conservation law of NP and NPZ models can be derived in a similar way.

According to equation (2.2), we obtain the conservation law by adding these differential equations:

$$\frac{d}{dt}(N + P + Z + D) = 0 \tag{2.12}$$

hence, the total biomass is conserved and we define it as

$$N_T = N + P + Z + D. \tag{2.13}$$

The total biomass, N_T, will be used in chapter 4 as a parameter we vary to observe different behaviors in the system. Note that the conservation law (2.12) can be used to express D in terms of the other variables and hence write (2.9) as an equivalent reduced system:

$$\begin{aligned}
\frac{dN(t)}{dt} &= -\nu P \frac{N}{N+1} + \alpha(N_T - N - P - Z) \\
\frac{dP(t)}{dt} &= \nu P \frac{N}{N+1} - \lambda P^m - gZ\frac{P}{P+1} \\
\frac{dZ(t)}{dt} &= gZ\frac{P}{P+1} - \delta Z \\
D(t) &= N_T - N(t) - P(t) - Z(t)
\end{aligned} \tag{2.14}$$

Given an initial condition for (3.21), the value of total biomass N_T will be fixed and the solution will evolve on the reduced system (2.14) for $t > 0$.

When we sum the PDE model (2.9), we obtain a different equation that is a diffusion type equation,

$$\frac{\partial}{\partial t}[N+P+Z+D] = \frac{\partial^2}{\partial x^2}[d_1 N + d_2 P + d_3 Z + d_4 D]$$

This can be integrated over the spatial domain and since we impose Neumann boundary conditions on all the species, we obtain

$$\frac{\partial}{\partial t}\int_0^{2\pi} [N+P+Z+D]\,dx = 0.$$

Therefore, we can still introduce a total biomass as we did in equation (2.13), but now it is the integral of the total biomass over the whole domain that is conserved,

$$\int_0^{2\pi} [N+P+Z+D]\,dx = \tilde{N}_T. \tag{2.15}$$

Chapter 3

Linear Stability Analysis

In this chapter, we introduce the general form of the linearization of models (2.3), (2.6) and (2.9), respectively. By comparing the stability of the same model with and without diffusions, we determine how the different diffusion coefficients d_i can affect the stability. We use this to formulate conditions for the existence of Turing instability.

Suppose we have a system of reaction diffusion equations as the following:

$$\frac{\partial Y(x,t)}{\partial t} = \mathcal{D}\nabla^2 Y(x,t) + f(Y) \tag{3.1}$$

where Y represents the vector of variable such as $Y = [N,P]^T, [N,P,Z]^T, [N,P,Z,D]^T$ and the spatially homogeneous equilibrium point Y^* is defined if $f(Y^*) = 0$.

In the absence of diffusion, we have the following form of linearization around the equilibrium points:

$$\frac{dW(t)}{dt} = J^*_{ode} W(t), \tag{3.2}$$

where we define $W(t)$ as the vector of perturbations of all biological concentrations from the equilibrium points ($[N(t)-N^*, P(t)-P^*, Z(t)-Z^*, D(t)-D^*]$ as an example) and J^*_{ode} is the Jacobian matrix with respect to the reaction terms of the models (2.3), (2.6) and (2.9) at the equilibrium points. We study the nature of equilibrium and J^*_{ode} in the later sections for NP, NPZ and $NPZD$ models, respectively.

In the presence of diffusion, we have the following form of linearization:

$$\frac{\partial W(x,t)}{\partial t} = J^*_{ode} W(x,t) + \mathcal{D}\nabla^2 W(x,t), \tag{3.3}$$

where $\mathcal{D}$ is the diagonal matrix with d_i in the corresponding diagonal positions.

Due to the Neumann boundary conditions, we assume a solution $W(x,t)$ in the following form:

$$W = \sum_k \exp(\lambda_k t)\cos(kx)v_k \tag{3.4}$$

Substituting this into equation (3.3) gives the eigenvalue problem

$$\lambda_k v_k = J^*_{pde} v_k,$$

where $J^*_{pde} = J^*_{ode} - k^2\mathcal{D}$ and λ_k, v_k is the eigen-pair of matrix J^*_{pde} with respect to k.

We have:

$$k \in \mathcal{K} = \{\frac{n}{2}, n \in Z\} \tag{3.5}$$

since the Neumann boundary conditions implies that $\cos(kx)$ has 0 gradient with respect to x on the boundary.

Notice that equation (3.4) is a sum over different wave numbers k. Each term in the sum is an eigenfunction and can grow exponentially and/or oscillate with respect to time. The nature of the eigenvalue λ_k determines the type of behavior.

Diffusion-driven instability was first introduced by Turing [27] and later discussed in detail by Murray [18]. Consider Equation (3.1) to define the conditions for a Turing instability. Let Y^* denote a homogeneous equilibrium satisfying $f(Y^*) = 0$. The equilibrium Y^* is said to exhibit a *Turing instability* if it is linearly stable in the absence of diffusion—i.e., all eigenvalues of the Jacobian J^*_{ode} have negative real parts—but becomes unstable for some spatial wavenumber $k > 0$ when diffusion is introduced. Formally, this occurs when at least one eigenvalue λ_k of the linearized reaction–diffusion Jacobian J^*_{pde} satisfies $\text{Re}(\lambda_k) > 0$. A spatial mode $\cos(kx)$ with wavenumber k is called an *unstable mode* if its associated eigenvalue λ_k of J^*_{pde} satisfies $\text{Re}(\lambda_k) > 0$.

Hence, the emergence of modes with $\text{Re}(\lambda_k) > 0$ due to diffusion indicates a Turing instability, where diffusion destabilizes an stable homogeneous steady state. We investigate the emergence of unstable modes of the form $\exp(\lambda_k t)$ over time. The instability arises for specific modes k with the corresponding growth rates determined by λ_k.

Our study combines analytical insights into Turing instability with numerical experiments that provide supporting evidence.

3.1 NP Model

This section analyzes the stability of the system both with and without diffusion. We investigate on how different magnitudes of diffusion coefficients might induce the Tur-

ing instability. The analysis is conducted using the specified forms of the reaction and death terms given by the following system:

$$\begin{aligned} \frac{\partial N}{\partial t} &= d_1 \frac{\partial^2 N}{\partial x^2} - \nu P \frac{N}{N+1} + \lambda P^m \\ \frac{\partial P}{\partial t} &= d_2 \frac{\partial^2 P}{\partial x^2} + \nu P \frac{N}{N+1} - \lambda P^m \end{aligned} \tag{3.6}$$

3.1.1 Equilibrium

The model (3.6) has 2 different types of spatially invariant equilibria. Let $[N^*, P^*]$ be an equilibrium of (3.6). Then N^*, P^*, Z^*, D^* must satisfy:

$$\begin{aligned} \nu P \frac{N}{N+1} &= \lambda P^m \\ N + P &= N_T \end{aligned} \tag{3.7}$$

.

Assume $P^* = 0$, this leads to the trivial equilibrium solution: $[N^*, P^*] = [N_T, 0]$.

For the non-trivial equilibrium case where $P^* \neq 0$, the equilibrium points $[N^*, P^*]$ are obtained by solving equation (3.7).

Table 3.1 shows the summarized information for different types of equilibrium in NP model.

Table 3.1: Types of equilibrium states in the NP model.

Type	**Equilibrium Form**
Trivial Equilibrium	$[N_T, 0]$
Co-existence Equilibrium	$[N^*, P^*]$

In our research, we focus on the co-existence equilibrium.

3.1.2 Stability without Diffusion

Without the spatial diffusion terms, we have:

$$\begin{aligned} \frac{dN}{dt} &= F(N,P) = -\nu P \frac{N}{N+1} + \lambda P^m \\ \frac{dP}{dt} &= G(N,P) = \nu P \frac{N}{N+1} - \lambda P^m \end{aligned} \tag{3.8}$$

Note that equilibria of these equations satisfy the same equations 3.7 as spatially invariant equilibria of the model with diffusion.

We define F and G as the reaction terms, F_N, F_P, G_N and G_P are the corresponding partial derivatives. The Jacobian matrix of the system (3.8) is:

$$J^*_{ode} = \begin{bmatrix} F_N & F_P \\ G_N & G_P \end{bmatrix} = \begin{bmatrix} -\nu P^* \frac{1}{(N^*+1)^2} & -\nu \frac{N^*}{N^*+1} + m\lambda (P^*)^{m-1} \\ \nu P^* \frac{1}{(N^*+1)^2} & \nu \frac{N^*}{N^*+1} - m\lambda (P^*)^{m-1} \end{bmatrix} = \begin{bmatrix} -\nu P^* \frac{1}{(N^*+1)^2} & (m-1)\lambda (P^*)^{m-1} \\ \nu P^* \frac{1}{(N+1)^2} & -(m-1)\lambda (P^*)^{m-1} \end{bmatrix} \tag{3.9}$$

with the corresponding characteristic polynomial:

$$p_{ode}(\lambda) = \lambda^2 + a_1 \lambda + a_0 = \lambda^2 + (-F_N - G_P)\lambda.$$

Thus the two eigenvalues are 0 and $F_N + G_P$.

Therefore, the system without diffusion (3.8) is linearly stable at the equilibrium points $[N^*, P^*]$ if and if only the trace $F_N + G_P = -\nu P \frac{1}{(N+1)^2} - (m-1)\lambda P^{m-1}$ of Jacobian J^*_{ode} is negative. Specifically, in a conservative system, the Jacobian matrix is not of full rank, which implies that its determinant is zero. Moreover, the constant term in the characteristic polynomial is $(-1)^n det(J^*_{ode})$, where n denotes the dimension of the matrix. Consequently, for a conservative NP system, we have $a_0 = 0$. Similar analysis can be extended to the nutrient–phytoplankton–zooplankton (NPZ) model and the nutrient–phytoplankton–zooplankton–detritus (NPZD) model.

More importantly, the NP model satisfies the conservation law $N + P = N_T$, the dynamics are restricted to the one-dimensional invariant subspace

$$M = \{(N, P) \in \mathbb{R}^2 : N + P = N_T\}.$$

The zero eigenvalue arises because motion in the direction normal to M is forbidden by the conservation law; it does not correspond to an unstable direction reflecting the fact that trajectories cannot leave the invariant subspace. Therefore, stability is determined solely by the nonzero eigenvalue of the Jacobian, which corresponds to perturbations tangent to the invariant subspace. If this eigenvalue has negative real part, the equilibrium is stable when restricted to M; if its real part is positive, the equilibrium is unstable on M. In this sense, the equilibrium is asymptotically stable within the invariant subspace but only stable in the full state space, due to the presence of the conservation-induced zero eigenvalue; similar arguments are discussed in the Chapter 2 of [24].

3.1.3 Diffusion induced Instability

According to the general analysis at the beginning of this section, the core to analyze the stability of diffusional system is to study the stability of matrix J^*_{pde} given by the

following definition.

$$J^*_{pde} = J^*_{ode} - k^2 D = \begin{bmatrix} F_N - d_1 k^2 & F_P \\ G_N & G_P - d_2 k^2 \end{bmatrix} = \begin{bmatrix} -\nu P \frac{1}{(N+1)^2} - d_1 k^2 & (m-1)\lambda P^{m-1} \\ \nu P \frac{1}{(N+1)^2} & -(m-1)\lambda P^{m-1} - d_2 k^2 \end{bmatrix}$$

with its corresponding characteristic polynomial:

$$p_{pde}(\lambda) = \lambda^2 + b_1 \lambda + b_0 = \lambda^2 + \Big((d_1 + d_2)k^2 - F_N - G_P\Big)\lambda + d_1 d_2 k^4 + k^2(-d_2 F_N - d_1 G_P).$$

In order to induce Turing instability, we assume the system without diffusion (3.8) is linearly stable at the equilibrium point $[N^*, P^*]$ and seek conditions under which the roots of $p_{pde}(\lambda)$ have positive real parts.

Based on the continuity of the quadratic, if $b_0 \cdot b_1 < 0$, the system with diffusion is unstable. In other words, if one of b_0 and b_1 is negative and the other is positive, and given that $-F_N - G_P > 0$, there is Turning instability. Moreover, since $b_1 = (d_1 + d_2)k^2 - F_N - G_P > 0$, the only way to induce Turing instability is to impose $b_0 < 0$ by varying the relative magnitudes of diffusion coefficients. b_0 is given by:

$$b_0 = d_1 d_2 k^4 + k^2(-d_2 F_N - d_1 G_P) \tag{3.10}$$

Notice that we have $F_N < 0$ and $G_P = -(m-1)\lambda P^{m-1}$. Moreover, $G_P > 0$ if and only if $0 < m < 1$. Therefore, we require $0 < m < 1$ otherwise $b_0 > 0$. In the numerical simulations, we set $m = \frac{1}{2}$. The rationale for this choice of m will be discussed later in Section 4.2.2.

Furthermore, let us consider how different magnitudes of d_1 and d_2 might induce Turing instability. Recall we need to ensure the condition $|F_N| > |G_P|$ from the stability condition of ODE system. $d_1 >> d_2$ could lead to $|d_1 G_P| >> |d_2 F_N|$, thus it is possible that $b_0 < 0$. For instance, if $|G_P| < |F_N| < 10 \cdot |G_P|$, we can set $d_1 > 100 \cdot d_2$, then $|d_1 G_P| > |d_2 F_N|$ given that $|F_N| > |G_P|$.

b_0 cannot be negative for all wave numbers k even if $-d_2 F_N - d_1 G_P \ll 0$ since the leading coefficient of k^4 is positive. Therefore, we expect Turing instability exist for a limited range of small k values, provided the following conditions. Furthermore, we expect Turing instability is harder to emerge for relatively large k.

$$\begin{aligned} &d_1 \gg d_2 \\ &d_2 \ll 1 \\ &0 < m < 1 \end{aligned} \tag{3.11}$$

Numerical simulations confirming that Turing instability can occur under these conditions are presented in section 4.2.3.

3.2 NPZ Model

This section analyzes the stability of the system both with and without diffusion. We investigate on how different magnitudes of diffusion coefficients might induce the Turing instability. The NPZ model with only the reaction part is given by:

$$\begin{aligned}
\frac{dN}{dt} &= F(N,P,Z) = -\nu P\frac{N}{N+1} + \lambda P^m + \delta Z \\
\frac{dP}{dt} &= G(N,P,Z) = \nu P\frac{N}{N+1} - \lambda P^m - gZ\frac{P}{P+1} \\
\frac{dZ}{dt} &= H(N,P,Z) = gZ\frac{P}{P+1} - \delta Z
\end{aligned} \tag{3.12}$$

3.2.1 Equilibrium

The NPZ model has 3 different types of equilibria.

Assuming $P^* = 0$, we obtain $Z^* = 0$. According to the conservation law, this gives $N^* = N_T$, resulting in the trivial equilibrium state:

$$[N^*, P^*, Z^*] = [N_T, 0, 0].$$

For the case $P^* \neq 0$ and $Z^* = 0$, we obtain the second type of equilibrium state:

$$[N^*, P^*, Z^*] = [N^*, P^*, 0],$$

which can be determined from the set of equations (3.7).

Finally, when both $P^* \neq 0$ and $Z^* \neq 0$, the system admits a third type of equilibrium state:

$$[N^*, P^*, Z^*] = [N^*, P^*, Z^*],$$

which can be obtained by solving the following equations:

$$\begin{aligned}
&\frac{P}{P+1} = \frac{\delta}{g} \\
&\nu P\frac{N}{N+1} = gZ\frac{P}{P+1} + \lambda P^m \\
&N + P + Z = N_T
\end{aligned} \tag{3.13}$$

After simplification, we obtain a quadratic equation solving the equilibrium point N^*:

$$N^{*2} + \left(1 + \frac{\nu+\delta}{g-\delta} - \frac{\lambda}{\delta}(\frac{\delta}{g-\delta})^m - N_T\right)N^* + \left(\frac{\delta}{g-\delta} - \frac{\lambda}{\delta}(\frac{\delta}{g-\delta})^m - N_T\right) = 0 \tag{3.14}$$

Table 3.2 gives a summarized information of different types of equilibrium:

Table 3.2: Types of equilibrium states in the NPZ model.

Type	Equilibrium Form
Trivial Equilibrium	$[N_T, 0, 0]$
Non-trivial Equilibrium	$[N^*, P^*, 0]$
Co-existence Equilibrium	$[N^*, P^*, Z^*]$

In our research, we focus on the co-existence equilibrium.

3.2.2 Stability without Diffusion

We define F, G and H as the reaction terms with the corresponding partial derivatives in the following Jacobian matrix J^*_{ode}:

$$J^*_{ode} = \begin{bmatrix} F_N & F_P & F_Z \\ G_N & G_P & G_Z \\ H_N & H_P & H_Z \end{bmatrix} = \begin{bmatrix} -\nu P^* \frac{1}{(1+N^*)^2} & -\nu \frac{N^*}{N^*+1} + \lambda m (P^*)^{m-1} & \delta \\ \nu P^* \frac{1}{(1+N^*)^2} & \nu \frac{N^*}{N^*+1} - \lambda m (P^*)^{m-1} - g Z^* \frac{1}{(1+P^*)^2} & -g \frac{P^*}{P^*+1} \\ 0 & g Z^* \frac{1}{(1+P^*)^2} & 0 \end{bmatrix}$$

with its corresponding characteristic polynomial being:

$$p_{ode}(\lambda) = \lambda^3 + a_2\lambda^2 + a_1\lambda + a_0$$

and coefficients are given by:

$$\begin{aligned} a_2 &= -Trace(J^*) = -(F_N + G_P) \\ a_1 &= -(M_1 + M_2 + M_3) = -(F_P G_N - F_N G_P + H_P G_Z) \\ a_0 &= -det(J^*) = 0 \end{aligned}$$

The conservation law implies that the corresponding Jacobian matrix J^*_{ode} is not of full rank, as its rows are linearly dependent. As a result, $\det(J^*_{ode}) = 0$ for the nutrient–phytoplankton–zooplankton model, so that the constant term $a_0 = -\det(J^*_{ode}) = 0$.

We can simplify the original characteristic polynomial as:

$$p_{ode}(\lambda) = \lambda(\lambda^2 + a_2\lambda + a_1)$$

Thus, the characteristic equation always possesses a zero eigenvalue. For the equilibrium point to be stable, all remaining eigenvalues must have negative real parts. By the continuity of the characteristic polynomial, and excluding the known zero eigenvalue, the following conditions guarantee that p_{ode} has all other roots with negative real parts:

$$\begin{aligned} a_1 &> 0 \\ a_2 &> 0. \end{aligned} \tag{3.15}$$

By analogy to the NP model, the NPZ system satisfies the conservation law $N+P+Z = N_T$, restricting dynamics to the two-dimensional invariant subspace

$$M = \{(N, P, Z) \in \mathbb{R}^3 : N + P + Z = N_T\}.$$

Stability is therefore determined by the nonzero eigenvalues of the J^*_{ode} restricted to M.

3.2.3 Diffusion induced Instability

Assuming that the system without diffusion (3.12) is stable at the equilibrium points $[N^*, P^*, Z^*]$ with condition (3.15), we can discuss the conditions for the instability of the system with diffusion:

$$\begin{aligned} \frac{\partial N}{\partial t} &= d_1 \frac{\partial^2 N}{\partial x^2} - \nu P \frac{N}{N+1} + \lambda P^m + \delta Z \\ \frac{dP}{dt} &= d_2 \frac{\partial^2 P}{\partial x^2} + \nu P \frac{N}{N+1} - \lambda P^m - gZ\frac{P}{P+1} \\ \frac{dZ}{dt} &= d_3 \frac{\partial^2 Z}{\partial x^2} + gZ\frac{P}{P+1} - \delta Z \end{aligned} \tag{3.16}$$

where the Jacobian J^*_{pde} and its characteristic polynomial is given by:

$$J^*_{pde} = J^*_{ode} - k^2 D = \begin{bmatrix} F_N - d_1 k^2 & F_P & F_Z \\ G_N & G_P - d_2 k^2 & G_Z \\ H_N & H_P & H_Z - d_3 k^2 \end{bmatrix} \tag{3.17}$$

$$p_{pde}(\lambda) = \lambda^3 + b_2\lambda^2 + b_1\lambda + b_0$$

The coefficients of $p_{pde}(\lambda)$ are given by:

$$
\begin{aligned}
b_2 &= a_2 + k^2(d_1 + d_2 + d_3) \\
b_1 &= a_1 - k^2(d_2 + d_3)F_N - k^2(d_1 + d_3)G_P - k^2(d_1 + d_2)H_Z + k^4(d_1d_2 + d_1d_3 + d_2d_3) \\
b_0 &= a_0 + d_1d_2d_3k^6 + (d_1d_2H_Z + d_1d_3G_P + d_2d_3F_N)k^4 \\
&\quad + d_1k^2(G_zH_P - G_PH_Z) + d_2k^2(F_ZH_N - F_NH_Z) + d_3k^2(F_PG_N - F_NG_P)
\end{aligned}
$$

The Routh array method provides a systematic procedure to test the stability of a linear system by examining the signs of the first-column elements derived from the characteristic polynomial coefficients according to the Routh–Hurwitz stability criterion [19]. If there are sign changes in the first column of the Routh array, the system is unstable. The Routh array is given by:

$$
\begin{array}{c|cc}
\lambda^3 & 1 & b_1 \\
\lambda^2 & b_2 & b_0 \\
\lambda^1 & (b_2b_1 - b_0)/b_2 & 0 \\
\lambda^0 & b_0 & 0
\end{array}
$$

Notice that if $b_0 < 0$ and leading coefficient $1 > 0$, no matter what the signs of the middle terms in the first column are, there is at least one sign changes in the first column. Therefore, $b_0 < 0$ ensures the system with diffusion (2.6) is unstable.

Simplify b_0 as a polynomial of k:

$$
\begin{aligned}
b_0 &= d_1d_2d_3k^6 - (d_1d_3G_P + d_2d_3F_N)k^4 \\
&\quad + d_1k^2\left(-g\delta Z\frac{1}{(1+P)^2} - \delta G_P\right) + d_3k^2(\nu P\frac{1}{(1+N)^2}(G_P - \nu P\frac{1}{(1+N)^2})).
\end{aligned}
\tag{3.18}
$$

Notice that the relative magnitudes of the coefficients associated with different powers of k determine the sign of b_0. Our objective is to determine conditions under which $b_0 < 0$ when the scales of diffusion coefficients d_1, d_2, and d_3 are adjusted appropriately.

The coefficient of k^6, namely $d_1d_2d_3$, is always positive. The coefficient of k^2, which involves d_1, becomes negative when $0 < m \leq 1$. By simplifying

$$
G_P = gZ\frac{1}{1+P}\frac{\delta}{g} + \lambda P^{m-1}(1-m),
$$

we find that $0 < m \leq 1$ is a sufficient condition for $G_P > 0$. Consequently, the term

$$
-g\delta Z\frac{1}{(1+P)^2} - \delta G_P
$$

is negative when $0 < m \leq 1$. Furthermore, if $d_1 \gg d_3$, the coefficient of term k^2 can be driven into the negative range in Equation (3.18).

Next, consider the coefficient of k^4. Given $0 < m \leq 1$, we have $H_Z = 0$, $F_N < 0$, and $G_P > 0$. If the diffusivity parameters satisfy $d_1 \gg d_2$, then

$$-(d_1 d_2 H_Z + d_1 d_3 G_P + d_2 d_3 F_N) = -(d_1 d_3 G_P + d_2 d_3 F_N) < 0. \tag{3.19}$$

As an illustrative example, if we have $10|G_P| < |F_N| < 100|G_P|$, we can choose $d_1 > 100\, d_2$ such that $|d_2 d_3 F_N| < |d_1 d_3 G_P|$. Therefore, there exists an appropriate set of diffusion coefficients so that equation (3.19) holds.

The above analysis suggests that under suitable parameter selection, the coefficients of the characteristic polynomial have the appropriate signs to support the necessary setting for diffusion-driven (Turing) instability to occur. In particular, sufficiently large contrasts between diffusion coefficients may destabilize the homogeneous steady state even when it is locally stable in the absence of diffusion.

Therefore, to support the possible emergence of Turing instability, we assume the following parameter conditions based on the preceding analysis:

$$\begin{aligned} d_1 &\gg d_3, d_2 \\ 0 &< m < 1 \end{aligned} \tag{3.20}$$

We can ensure that the coefficients of k^4 is negative. The additional condition $1 \gg d_2, d_3$ is imposed to guarantee that the positive coefficient $d_1 d_2 d_3$ of k^6 remains smaller in magnitude than the coefficients of k^2 and k^4, respectively. It should be emphasized that this condition is intended only to provide intuition for achieving negativity of b_0 for a certain range of wavenumbers k; it does not imply that the condition is sufficient to induce Turing instability. Furthermore, this reasoning may fail for sufficiently large k, as the leading coefficient of the highest power, k^6, is positive.

A more detailed numerical verification, along with intuition on the choice of diffusion parameters and m is provided later in Section 4.3.3.

3.3 NPZD Model

According to [12], an NPZ model with time delayed nutrient recycling can be equivalent to an ODE model with an added detritus compartment, called an NPZD model:

$$
\begin{aligned}
\frac{dN}{dt} &= -\nu P\frac{N}{N+1} + \alpha D \\
\frac{dP}{dt} &= \nu P\frac{N}{N+1} - \lambda P^m - gZ\frac{P}{P+1} \\
\frac{dZ}{dt} &= gZ\frac{P}{P+1} - \delta Z \\
\frac{dD}{dt} &= \lambda P^m + \delta Z - \alpha D
\end{aligned}
\tag{3.21}
$$

3.3.1 Equilibrium

The model (3.21) can admit three types of equilibria. Let $[N^*, P^*, Z^*, D^*]$ be an equilibrium of (3.21). Then N^*, P^*, Z^*, D^* must satisfy

$$
\begin{aligned}
-\nu P\frac{N}{N+1} + \alpha D &= 0 \\
P\left(\nu\frac{N}{N+1} - \lambda P^{m-1} - gZ\frac{1}{P+1}\right) &= 0 \\
Z\left(g\frac{P}{P+1} - \delta\right) &= 0 \\
N + P + Z + D &= N_T
\end{aligned}
\tag{3.22}
$$

Assume $P^* = 0$, then $D^* = Z^* = 0$, so that $N^* = N_T$ which leads to the first type of equilibrium: the trivial equilibrium $[N_T, 0, 0, 0]$.

Assuming $P^* \neq 0$ and $Z^* = 0$, leads to the second type of equilibrium $[N^*, P^*, 0, D^*]$ given by solving the following relations:

$$
\begin{aligned}
\nu P\frac{N}{N+1} &= \lambda P^m = \alpha D \\
N + P + D &= N_T
\end{aligned}
$$

When $P^*, Z^* \neq 0$, we have the third type of equilibrium point $[N^*, P^*, Z^*, D^*]$ which the focus of our research. The following equations from the ODE model is used to solve the third type equilibrium:

$$\frac{P}{P+1} = \frac{\delta}{g} \tag{3.23}$$

$$Z = \frac{\nu}{\delta}\frac{\delta}{g-\delta}\frac{N}{N+1} - \frac{\lambda}{\delta}\left(\frac{\delta}{g-\delta}\right)^m \tag{3.24}$$

$$D = \frac{\nu}{\alpha}\frac{\delta}{g-\delta}\frac{N}{N+1} \tag{3.25}$$

$$N + P + Z + D = N_T \tag{3.26}$$

Using this and the representations of Z^* and D^* in terms of N^*, we have the following quadratic equation for N^*:

$$N^{*2} + \left(1 + \frac{\nu}{\alpha}\frac{\delta}{g-\delta} + \frac{\nu+\delta}{g-\delta} - \frac{\lambda}{\delta}(\frac{\delta}{g-\delta})^m - N_T\right)N^* + \left(\frac{\delta}{g-\delta} - \frac{\lambda}{\delta}(\frac{\delta}{g-\delta})^m - N_T\right) = 0 \tag{3.27}$$

Table 3.3 gives a summarized information of different types of equilibrium:

Table 3.3: Types of equilibrium states in the $NPZD$ model.

Type	Equilibrium Form
Trivial Equilibrium	$[N_T, 0, 0, 0]$
Non-trivial Equilibrium	$[N^*, P^*, 0, D^*]$
Co-existence	$[N^*, P^*, Z^*, D^*]$

In our research, we focus on the co-existence equilibrium.

3.3.2 Stability without Diffusion

The Jacobian of the NPZD model without diffusion (3.21) is given by:

$$J^*_{ode} = \begin{bmatrix} -\nu P^* \frac{1}{(1+N^*)^2} & -\nu \frac{N^*}{N^*+1} & 0 & \alpha \\ \nu P^* \frac{1}{(1+N^*)^2} & \nu \frac{N^*}{N^*+1} - \lambda m (P^*)^{m-1} - gZ^* \frac{1}{(1+P^*)^2} & -g\frac{P^*}{P^*+1} & 0 \\ 0 & gZ^* \frac{1}{(1+P^*)^2} & 0 & 0 \\ 0 & \lambda m (P^*)^{m-1} & \delta & -\alpha \end{bmatrix} \tag{3.28}$$

with the corresponding characteristic polynomial:

$$p_{ode}(\lambda) = \lambda^4 + a_3\lambda^3 + a_2\lambda^2 + a_1\lambda + a_0$$

It is helpful for us to simplify the Jacobian before we proceed to discuss the stability of PDE system as there are lots of repeated terms in the Jacobian. The ODE Jacobian can be expressed in the following form:

$$J^*_{ode} = \begin{bmatrix} -A & -B & 0 & E \\ A & B-C-F & -G & 0 \\ 0 & F & 0 & 0 \\ 0 & C & G & -E \end{bmatrix} \tag{3.29}$$

where we define

$$A = \nu P^* \frac{1}{(N^*+1)^2},\ B = \nu \frac{N^*}{N^*+1},\ C = \lambda m (P^*)^{m-1},$$
$$F = gZ^* \frac{1}{(P^*+1)^2},\ E = \alpha,\ G = \delta = g\frac{P^*}{P^*+1}.$$

Note that these are all positive constants.

The coefficients of the characteristic polynomial are represented by the following:

$$\begin{aligned} a_0 &= ADEG - ADEG = 0 \\ a_1 &= AFE + AFG + FEG \\ a_2 &= AC + AF + AE - BE + CE + FE + FG \\ a_3 &= A - B + C + F + E \end{aligned}$$

The vanishing of a_0, which is the determinant of the Jacobian, is a consequence of the fact the model has a conservation law. This means that the characteristic equation simplifies as follows:

$$p_{ode}(\lambda) = \lambda(\lambda^3 + a_3\lambda^2 + a_2\lambda + a_1). \tag{3.30}$$

Thus, the characteristic equation always has a zero root. For the equilibrium point to be stable, the rest of the eigenvalues must have a negative real part. Use the following Routh array [19] to discuss the roots of p_{ode}:

$$\begin{array}{c|cc} \lambda^3 & 1 & a_2 \\ \lambda^2 & a_3 & a_1 \\ \lambda^1 & (a_3a_2 - a_1)/a_3 & 0 \\ \lambda^0 & a_1 & 0 \end{array}$$

The Routh–Hurwitz stability criterion [19] states that if there is no sign changes in the first column of Routh array, then the system is stable. Therefore, the following conditions ensure the NPZD model with diffusion is stable:

$$\begin{aligned} a_1 &> 0 \\ a_3 &> 0 \\ a_2 a_3 - a_1 &> 0 \end{aligned} \tag{3.31}$$

The conditions (3.31) guarantee the equilibrium point is asymptotically stable in the reduced system.

A complete analysis of the signs of the coefficients is not possible. However, we note that $a_1 > 0$ and the condition $A - B + C + F > 0$ will guarantee both $a_2 > 0$ and $a_3 > 0$.

Furthermore, by analogy to the NP and NPZ model, the NPZD system satisfies the conservation law $N + P + Z + D = N_T$, restricting dynamics to the two-dimensional invariant subspace

$$M = \{(N, P, Z, D) \in \mathbb{R}^4 : N + P + Z + D = N_T\}.$$

Stability is therefore determined by the nonzero eigenvalues of the J^*_{ode} restricted to M.

3.3.3 Diffusion induced Instability

The simplified version of the J^*_{pde} is given by:

$$J^*_{pde} = J^*_{ode} - k^2 D = \begin{bmatrix} -A - d_1 k^2 & -B & 0 & E \\ A & B - C - F - d_2 k^2 & -G & 0 \\ 0 & F & -d_3 k^2 & 0 \\ 0 & C & G & -E - d_4 k^2 \end{bmatrix} \tag{3.32}$$

with the characteristic polynomial being:

$$p_{pde}(\lambda) = \lambda^4 + b_3 \lambda^3 + b_2 \lambda^2 + b_1 \lambda + b_0 \tag{3.33}$$

and the corresponding coefficients of the characteristic polynomial:

$$
\begin{aligned}
b_0 =& k^2(ADEd_3 + ADGd_4 + DEGd_1) \\
&+ k^4\Big(ACd_3d_4 + ADd_3d_4 + AEd_2d_3 - BEd_1d_3 + CEd_1d_3 + DEd_1d_3 + DGd_1d_4\Big) \\
&+ k^6\Big(Ad_2d_3d_4 - Bd_1d_3d_4 + Cd_1d_3d_4 + Dd_1d_3d_4 + Ed_1d_2d_3\Big) \\
&+ k^8 d_1d_2d_3d_4 \\
b_1 =& a_1 + k^2\Big(d_1(CE + DE + DG - BE) + d_2AE + d_3(AC + AD + AE - BE + CE + DE) + d_4(AC + AD + DG)\Big) \\
&+ k^4\Big(d_1d_3(C + D + E - B) + d_2d_3(A + E) + d_3d_4(A + C + D - B) + d_1d_4(C + D - B) + d_1d_2E + d_2d_4A\Big) \\
&+ k^6(d_1d_2d_3 + d_1d_2d_4 + d_2d_3d_4 + d_1d_3d_4) \\
b_2 =& a_2 + k^2\Big(d_1(C + D + E - B) + d_2(A + E) + d_3(A + C + D + E - B) + d_4(A + C + D - B)\Big) \\
&+ k^4(d_1d_2 + d_1d_3 + d_1d_4 + d_2d_3 + d_2d_4 + d_3d_4) \\
b_3 =& a_3 + k^2(d_1 + d_2 + d_3 + d_4)
\end{aligned}
$$

Since we are interested in Turing Instability, we focus on how the presence of different diffusion constants may induce instability of the equilibrium point, given that it is stable for the system without diffusion, i.e., that conditions (3.31) hold. To determine conditions for instability, we will apply the Routh–Hurwitz stability criterion [19]. Consider the first column of the Routh array:

$$
\begin{array}{c|ccc}
\lambda^4 & 1 & b_2 & b_0 \\
\lambda^3 & b_3 & b_1 & 0 \\
\lambda^2 & \dfrac{b_3b_2 - b_1}{b_3} & \dfrac{b_3b_0}{b_3} & 0 \\
\lambda^1 & \cdots & 0 & 0 \\
\lambda^0 & b_0 & &
\end{array}
$$

If $b_0 < 0$, then b_0 and the leading coefficient $1 > 0$ have opposite signs. So the equilibrium point in the system with diffusion is unstable if $b_0 < 0$ according to the Routh–Hurwitz stability criterion [19].

In the expression for b_0, note that the coefficients of k^2 and k^8 are positive, thus $b_0 < 0$ will only be possible if the coefficients of k^4 and/or k^6 are negative. These coefficients

are as follows:

$$\begin{aligned} k^4 &: ACd_3d_4 + ADd_3d_4 + AEd_2d_3 + (-B + C + F)Ed_1d_3 + FGd_1d_4 \\ k^6 &: Ad_2d_3d_4 + (-B + C + F)d_1d_3d_4 + Ed_1d_2d_3 \end{aligned} \tag{3.34}$$

Assume the following condition:

$$d_1 \gg d_3 \gg d_4 \gg d_2. \tag{3.35}$$

Then the coefficients are dominated by the following terms:

$$\begin{aligned} k^4 &: (-B + C + F)Ed_1d_3 \\ k^6 &: (-B + C + F)d_1d_3d_4 + Ed_1d_2d_3 \end{aligned} \tag{3.36}$$

and if $-B + C + F < 0$ then the coefficient of k^4 will be negative. Thus, instability is possible if the terms k^4 dominate in b_0, i.e., k is not too small or too large.

Finally, we consider the term $-B + C + F$. Using the equations for the equilibrium (3.22), we have

$$\begin{aligned} B - C - F &= \nu \frac{N^*}{N^* + 1} - \lambda m (P^*)^{m-1} - gZ^* \frac{1}{(1 + P^*)^2} \\ &= \lambda (P^*)^{m-1} + gZ^* \frac{1}{P^* + 1} - \lambda m (P^*)^{m-1} - gZ^* \frac{1}{(1 + P^*)^2} \\ &= (1 - m)\lambda (P^*)^{m-1} + gZ \frac{P^*}{(1 + P^*)^2} \end{aligned}$$

Thus if $m \leq 1$ then $-B + C + F < 0$ *for any* values of the other parameters.

In summary we have the following. For any values of the ODE model parameters with $m \leq 1$ and satisfying eq. (3.31), Turing instability is possible if the diffusion constants satisfy (3.35). In the next chapter we will use this analysis to find parameter values such that Turing instability occurs and numerically study the influence of the several parameters on this instability.

Chapter 4

Results

4.1 Numerical Methods

Our numerical studies are carried out using `Julia` [4]. The package `LinearAlgebra` is employed for the numerical solution of eigenvalue problems associated with the NP, NPZ, and NPZD models. To provide numerical evidence of Turing instability, we perform direct simulations of the corresponding PDE systems using the `Oceananigans` package [5], which provides a high-performance finite-volume solver for nonhydrostatic ocean models.

The computational domain is discretized on a rectilinear staggered grid with 64 points in the vertical direction. The grid topology is set as `(Flat, Flat, Bounded)`, indicating no spatial variation in x and y (a single vertical column), while the z-direction is bounded with physical boundary conditions at the top and bottom. This configuration concentrates resolution in the vertical direction, enabling accurate representation of stratification and tracer transport.

Time integration is performed using a third-order Runge–Kutta scheme. To ensure stability according to the Courant–Friedrichs–Lewy (CFL) condition [6], the time step is defined as

$$\Delta t = 0.1 \cdot \frac{(\Delta z)^2}{d_1},$$

where Δz is the vertical grid spacing size and d_1 is the largest diffusivity coefficient in the system.

All simulations are performed using the `NonhydrostaticModel` configuration of `Oceananigans` on the CPU backend.

4.1.1 Parameter

The parameter values used in the numerical simulations are listed in Tables 4.1, 4.2, and 4.3. These values, including ν, λ, δ, and g, are adopted from [12]. The selection of the total biomass N_T and the parameter m is discussed in Sections 4.2.2, 4.3.2, and 4.4.2. The diffusion coefficients are chosen to satisfy the conditions given in Equations (3.11), (3.20), and (3.35). The parameter σ denotes the standard deviation of the normally distributed random variable used as the initial condition; its value is selected to be relatively small compared with the magnitude of the equilibrium state in each model.

Although we also explored expressing the model in a non-dimensional form and considered the corresponding non-dimensional numbers, we ultimately chose to present the results in dimensional terms for clarity.

Parameter	Symbol	Value
Total conservative population	N_T	0.4
Interacting Coefficient of P and N	ν	5.9
death rate for P	λ	0.017
Power of death rate of P	m	$\frac{1}{2}$
Diffusion Coefficient of Nutrient	d_1	1
Diffusion Coefficient of Phytoplankton	d_2	0.0001
Standard Deviation of Normal Distribution	σ	10^{-5}

Table 4.1: NP Model Parameter

Parameter	Symbol	Value
Total conservative population	N_T	0.4
Interacting Coefficient of P and N	ν	5.9
death rate for P	λ	0.017
death rate of Z	δ	0.17
Interacting Coefficient of P and Z	g	7
Power of death rate of P	m	$\frac{1}{2}$
Diffusion Coefficient of Nutrient	d_1	5
Diffusion Coefficient of Phytoplankton	d_2	0.001
Diffusion Coefficient of Zooplankton	d_3	0.001
Standard Deviation of Normal Distribution	σ	0.0001

Table 4.2: NPZ Model Parameter

Parameter	Symbol	Value
Total conservative population	N_T	0.4
Interacting Coefficient of P and N	ν	5.9
death rate for P	λ	0.017
death rate of Z	δ	0.17
Transition rate of Detritus	α	1
Interacting Coefficient of P and Z	g	7
Power of death rate of P	m	$\frac{1}{2}$
Diffusion Coefficient of Nutrient	d_1	1
Diffusion Coefficient of Phytoplankton	d_2	0.0001
Diffusion Coefficient of Zooplankton	d_3	0.001
Diffusion Coefficient of Detritus	d_4	0.0001

Table 4.3: NPZD Model Parameter

4.2 NP Model

4.2.1 Stability Without Diffusion

In this section, we study numerically the stability of the NP model without diffusion. Recall from section 3.1 that the NP model without diffusion (3.8) is stable if and only if the trace of Jacobian J^*_{ode}, is negative

$$F_N + G_P = -\nu P^* \frac{1}{(N^*+1)^2} - (m-1)\lambda (P^*)^{m-1}.$$

Recall that the nontrivial equilibrium $[N^*, P^*]$ is determined by the total biomass parameter N_T, from equation (3.7). Furthermore, we have shown that $0 < m < 1$ is necessary to induce Turing instability for the NP model in section 3.1. $0 < m < 1$ implies $G_P > 0$ but $F_N < 0$ so that the sign of $F_N + G_P$ is uncertain when $0 < m < 1$. Therefore, the value of N_T thus affects the stability of the NP model without diffusion.

To make sure the selection of total biomass N_T ensuring the stability of NP model without diffusion, we fixed the the model parameter to be what is shown in Table 4.1, and choose a range of values for the total biomass, N_T. We numerically solved the equilibrium equations (3.7) at each value of N_T and calculated eigenvalues of the Jacobian of the linearization. We find that the largest real part of eigenvalues are close to machine precision, i.e., effectively 0, for each N_T ranging from 0.1 to 1 with a step size of 0.01. Recall that we always have an zero eigenvalue in our NP model by the conservation law. This means the nontrivial equilibrium point of the NP model without diffusion is stable

for each N_T from 0.1 to 1 when $m = \frac{1}{2}$. We choose $N_T = 0.4$ as the value for total biomass according to the discussion on Figure 4.1.

With this value, the equilibrium point is

$$[N^*, P^*]^T \approx [0.0046,\ 0.3954]^T.$$

4.2.2 Diffusion Induced Instability

In this section, we continue our discussion on the selection of total biomass N_T and the diffusion parameters d_1, d_2. Referring to the analysis in section 3.1, the diffusion induced instability might occur when $d_1 >> d_2$. We thus fix $d_1 = 1$ and vary d_2 from small values to large values to see the emergence of instability when d_2 decreases.

Figure 4.1 shows the linear growth rate of diffusional system with a range of total biomass values N_T and d_2 for $k = 1, 2, 4, 8$. The red color represents larger growth rate compared to blue color.

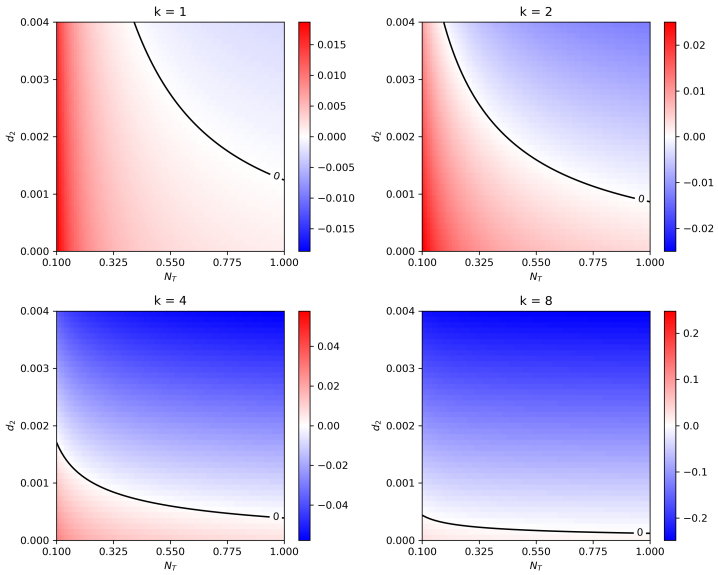


Figure 4.1: Dependence of linear growth rate of PDE model (2.3) on total biomass N_T and phytoplankton diffusion rate d_2 for modes k as shown. Other parameters values are given in Table 4.1

We can see that the smaller the total biomass N_T and the diffusion coefficient d_2, the larger the linear growth rate in Figure 4.1. This means that restricting the selection

of total biomass to be sufficient small will make the instability grow faster and thus be easier to see in a numerical simulation. However, if N_T is too small, then the magnitudes of the equilibrium N^*, P^* will also be small. This will further restrict the selection of magnitudes of initial perturbation which is discussed in the section 4.2.3.

Recall from the end of section 3.1.3 that it is harder for the Turing instability to occur for a large wave number k. This can be seen in Figure 4.1 that the bright area (area for the emergence of diffusion induced instability) decreases when wave number k increases from 2 to 4 to 8. Moreover, Figure 4.1 shows that the intuition from condition (3.11) is correct $d_1 = 1 \gg d_2$, specifically. Therefore, we fix $N_T = 0.4$ and $d_2 = 0.0001$ to further study the Turing instability. The largest real part, and hence strongest instability, is associated with $k = 4$ when $m = \frac{1}{2}$. See Figure 4.2.

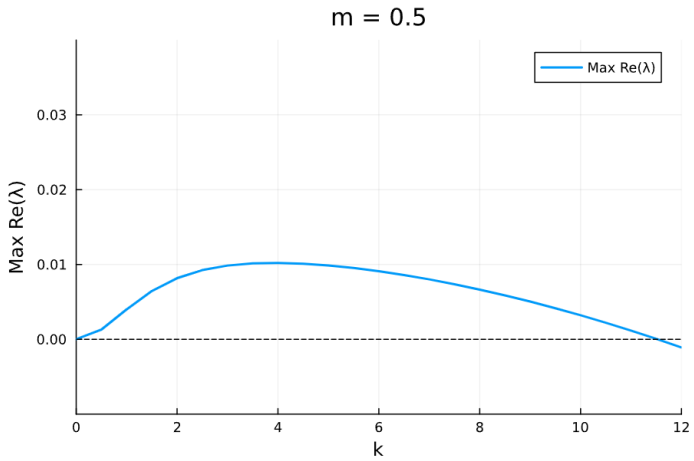


Figure 4.2: Dependence of linear growth rate of PDE model (2.3) on wave number k with $m = 0.5$. All other parameter values can be found in Table 4.1.

In section 3.1, we showed that $0 < m < 1$ is necessary for the emergence of Turing instability for NP model. Since our selection of $m = \frac{1}{2}$ is not a common choice of death rate power of P, we explore the effect of the parameters m and k on diffusion induced instability. Figure 4.3 visualizes the diffusion induced instability for various wave numbers k and values of m when $d_2 = 0.0001$. From this figure, it is clear that decreasing m has a destabilizing effect on the model. More importantly, for the parameters we consider, it is not possible to get a Turing instability with m much larger than 0.9. The figure only shows modes up to k = 22, but the trend for larger k is clear.

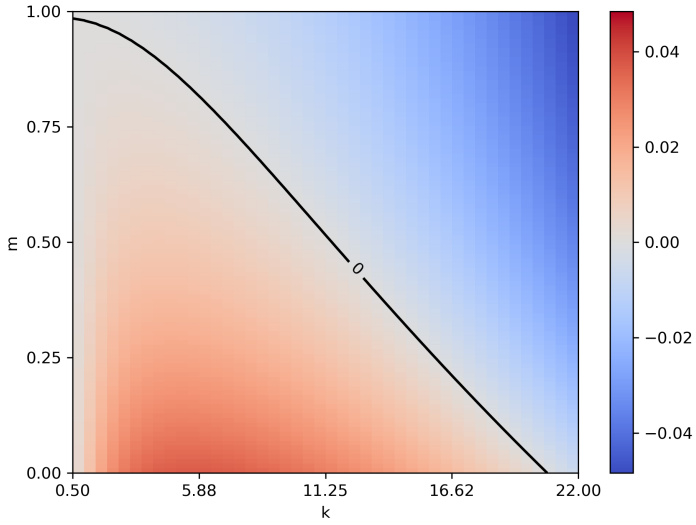


Figure 4.3: Dependence of linear growth rate of PDE model (2.3) on wave number k and phytoplankton mortality power m. All other parameter values can be found in Table 4.1.

4.2.3 Nonlinear simulations

In this section, results of simulations of the full nonlinear model (3.6) are presented. We will show that Turing instability does occur and verify that the linear growth rate in the simulations is as predicted by the linear stability analysis. The initial conditions are chosen to be perturbations from the equilibrium point:

$$[N,P](x,0) = [N^*,P^*] + [W_1,W_2](x),\ x \in [0,2\pi]. \tag{4.1}$$

We consider two choices for the perturbation functions: a single mode $\cos(4x)$ and random. The former is used to verify the linear growth of a single mode. The latter is to show the emergence of instability by a combination of various modes.

Mode $k = 4$

Figure 4.2 shows that for the parameters we consider, the largest linear growth rate of the PDE system corresponds to the mode $k = 4$. Thus we take the initial perturbation function in the form

$$W_j(x) = c\cos(4\pi)\,v_{4j}, \tag{4.2}$$

where the v_4 is the eigenvector associated with the eigenvalue with positive real part for $k = 4$ and c is a scaling factor to control the magnitude of initial perturbation compared to the magnitude of equilibrium $[N^*, P^*]$.

We want to make sure $|N^*|, |P^*| \gg |W_1|, |W_2|$.

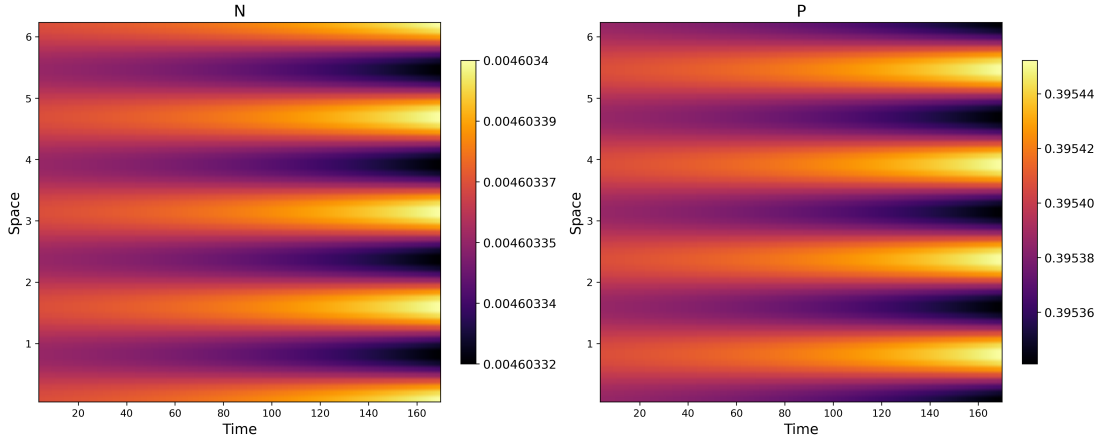


Figure 4.4: Evolution of NP model after initial perturbation with $k = 4$ mode

For values corresponding to the blue region of the $k = 4$ plot in Figure 4.1, the solution decays back to the steady state. An example with $d_2 = 0.004$ can be found in Figure A.1. Note from Figure 4.1 that there are unstable modes for this value of d_2 when $k = 2, 4, 8$ and $N_T = 0.4$. For values corresponding to the red region of the $k = 4$ plot in Figure 4.1, the solution grows. An example is shown in Figure 4.4 when $d_2 = 0.0001$. Note that the $k = 4$ mode structure of the solution is clearly visible at the end of the simulation.

As a simple check of our numerical method, we estimate the linear growth rate for this simulation. To do this we fit a line to the norm of the difference between the simulation results for each species and the corresponding equilibrium point. See Figure A.2 for an example. For each species, this fitted linear growth rate matched the real part of the eigenvalue to two decimal places. Moreover, we apply a Fourier decomposition to the numerical perturbation and plot the corresponding power spectrum in Figure A.3. We can see that there is only one mode, $k = 4$, that appears in the figure.

Random initial condition

Next, we consider simulations with a more realistic initial condition, the random initial condition, compared to the single mode initial condition. The random initial condition

can be decomposed into a combination of different modes, unstable or stable modes. We consider initial conditions in the form (4.1) with $W_j(x)$ randomly generated. See the following definition:

$$W_j(x) = \epsilon_j(x), \quad \epsilon_j(x) \sim \mathcal{N}(0, \sigma^2) \tag{4.3}$$

where ϵ_j is a random variable which follows a normal distribution with standard deviation σ. We choose $\sigma = 10^{-4}$ in all the simulations for NP model.

An example with $d_1 = d_2 = 1$ is shown in Figure A.4 which shows the solution decaying to the steady state. This gives evidence that there are no unstable modes for this value of d_2.

A random initial condition will excite all the modes, but only the unstable modes will grow and induce instabilities based on Figure 4.2. We can see the spatial perturbations are evolving in time from Figure 4.5.

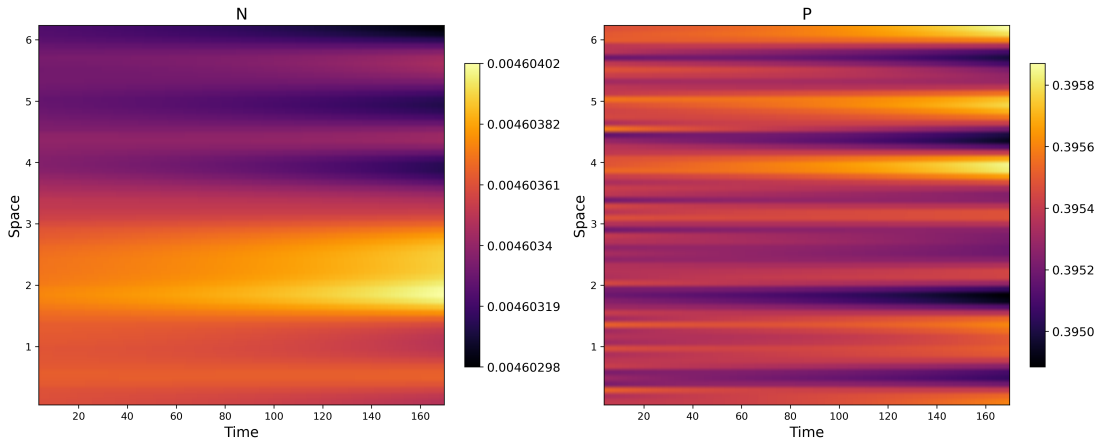


Figure 4.5: Evolution of NP model with random initial perturbation

To better understand diffusion induced instability from a random initial condition, we present the Fourier decomposition based on Figure 4.5. We can see the time emergence of the modes in Figure A.5. The decomposition of N contains modes with small wave numbers k from 1 to 3 and the decomposition of P contains a wide range of modes.

4.3 NPZ Model

In this section, we use numerical results to discuss the NPZ model both with and without diffusion. According to our analysis in section 3.2, we know that total biomass N_T

as a parameter affects the stability of equilibrium points of the NPZ model without diffusion. Therefore, we also discuss the selection of N_T in terms of affecting the stability in the NPZ model with diffusion.

Moreover, the selection of m and d_1 also affects the emergence of diffusion induced instability from our analysis according to conditions (3.20). Therefore, this section aims to study the selection of parameters.

4.3.1 Stability Without Diffusion

To study how N_T affects stability without diffusion, we fix the rest of the parameter according to Table 4.2 and choose a range of values of N_T. We numerically solved the equilibrium equations (3.13) using (3.14) at each value of N_T. Then we calculate the eigenvalues of the Jacobian of the linearization evaluated at the equilibrium point.

We can see in Figure 4.6 that an eigenvalue with a positive real part emerges when $N_T \approx 0.5$. To study the Turing instability we therefore need to take $N_T < 0.5$. Thus, we choose $N_T = 0.4$ as the value for our numerical simulations. The reason why the total biomass N_T is chosen as large as possible is discussed later in the Section 4.3.2. With this value, the equilibrium point is

$$[N^*, P^*, Z^*]^T \approx [0.2296,\ 0.0246,\ 0.1454]^T.$$

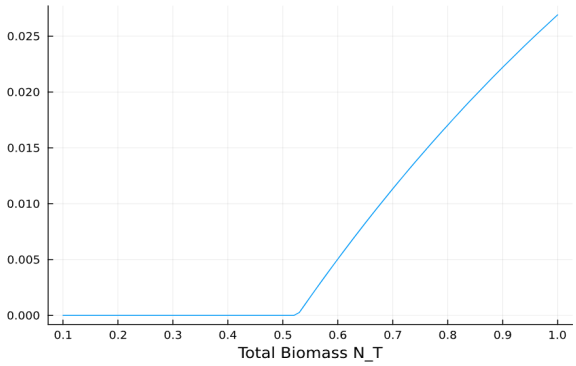


Figure 4.6: Dependence of linear growth rate of the ODE system (3.12) on the total biomass, N_T. Other parameter values are given in Table 4.2.

4.3.2 Diffusion Induced Instability

In this section, we continue our discussion of the selection of parameters, focusing on total biomass N_T and the nutrient diffusion constant d_1. Referring to the analysis in section 3.2, the diffusion induced instability might occur according to condition (3.20). Thus, we fix $d_2 = d_3 = 0.001$ and study the emergence of instability when d_1 increases.

Figure 4.7 shows the linear growth rate of the diffusion model with a range of values of N_T and d_1 for $k = 1, 2, 4, 6$.

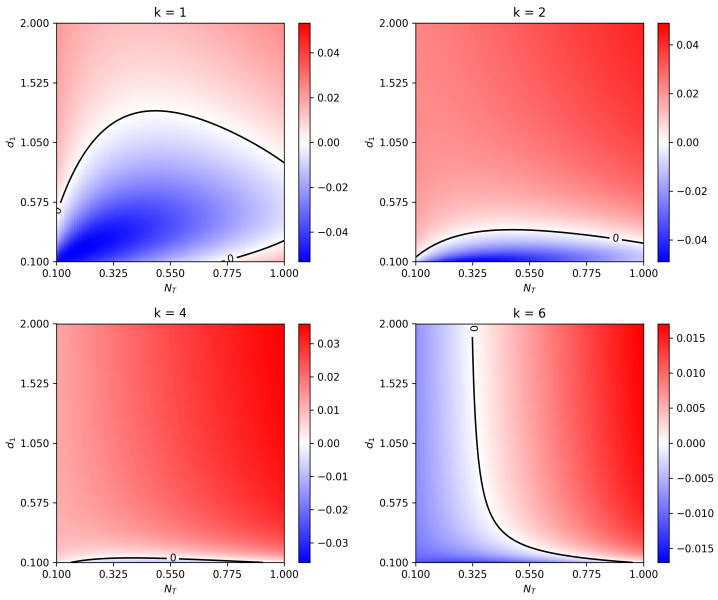


Figure 4.7: Dependence of linear growth rate of PDE model (2.6) on total biomass N_T and nutrient diffusion rate d_1 for modes k as shown. Other parameters values are given in Table 4.2.

Recall from Figure 4.6 that $N_T < 0.5$ ensures the stability of the NPZ model without diffusion. However, Figure 4.7 shows that the larger the total biomass N_T, the stronger the diffusion induced instabilities for $k = 1, 2, 4, 6$. We would like to pick N_T as large as possible to see the instability evolve quickly in the simulation. Therefore, we choose $N_T = 0.4$ in our simulations.

Moreover, Figure 4.7 shows that the intuition from condition (3.20) is correct $d_1 = 1 \gg d_2$, specifically as the color of the linear growth of the instability is brighter for larger values d_1. The largest real part, and hence the strongest instability, is associated with $k = 2$ when $m = \frac{1}{2}$. See Figure 4.8.

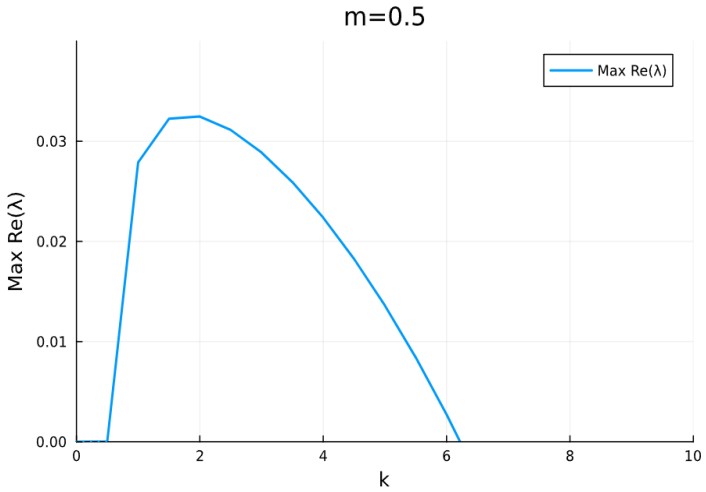


Figure 4.8: Dependence of linear growth rate of PDE model (2.6) on wave number k with $m = 0.5$. Other parameters values are given in Table 4.2.

Furthermore, we can see in Figure 4.7 that the blue region (stability) becomes larger when we increase the wave number k from 4 to 6. This validates the analysis in the end of section 3.2 that Turing instability can occur only for a certain set of wave number k and is expected to fail for large k. Figure 4.8 can also reveal the fact that the equilibrium of PDE system is stable with respect to perturbations with sufficiently large wave number k.

In section 3.2, we showed that $0 < m < 1$ is necessary for the emergence of Turing instability for NPZ model. since our selection of $m = \frac{1}{2}$ is not a common choice of the death rate power of P. We therefore explore some effects of various selections of m and k in Figure 4.9. Figure 4.9 visualizes the relationship between diffusion induced instability with various wave numbers k and m when $d_1 = 5$. From this figure it is clear that decreasing m has a destabilizing effect in the model. More importantly, for the parameters we consider, it is not possible to get a Turing instability with m much larger than 1. The figure only shows modes up to k = 15, but the trend for larger k is clear.

4.3.3 Nonlinear Simulations

In this section, results of simulations of the full nonlinear model (2.6) are presented. We will show that Turing instability does occur and verify that the linear growth rate in the simulations is as predicted by the linear stability analysis. The initial conditions

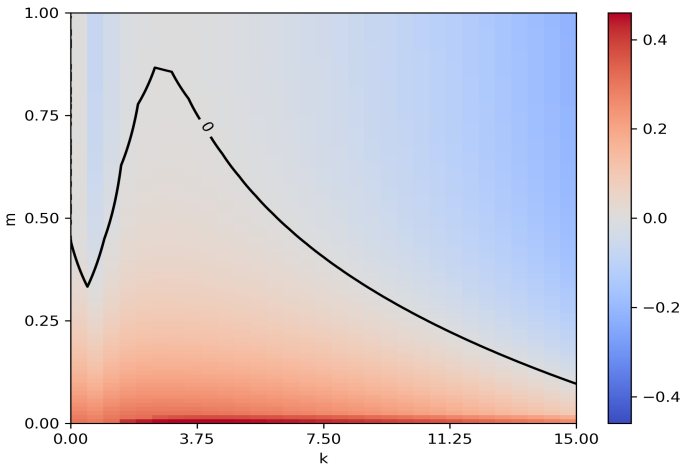


Figure 4.9: Dependence of linear growth rate of PDE model (2.6) on wave number k and phytoplankton mortaility power m. Other parameters values are given in Table 4.2.

are set up as perturbations from the equilibrium point:

$$[N,P,Z](x,0) = [N^*,P^*,Z^*] + [W_1,W_2,W_3](x),\ x \in [0,2\pi]. \tag{4.4}$$

We consider two choices for the perturbation functions: a single mode $\cos(2x)$ and random. The former is used to verify the linear growth of a single mode. The latter is to show the emergence of instability by a combination of various modes.

Mode $k = 2$

We take the initial perturbation function in the form

$$W_j(x) = c\cos(2\pi)\,v_{2j}, \tag{4.5}$$

where v_2 is the eigenvector associated with the eigenvalue with a positive real part for $k = 2$ and c is a scaling factor to control the magnitude of initial perturbation compared to the magnitude of equilibrium $[N^*,P^*,Z^*]$.

For values corresponding to the blue region of the $k = 2$ plot in Figure 4.7, the solution decays back to the steady state. An example can be found in Figure A.6 when $d_1 = 0.1$. For values corresponding to the red region in Figure 4.7, the solution grows. An example is shown in Figure 4.10 for $d_1 = 5$. Note that the $k = 2$ mode structure of the solution is clearly visible at the end of the simulation.

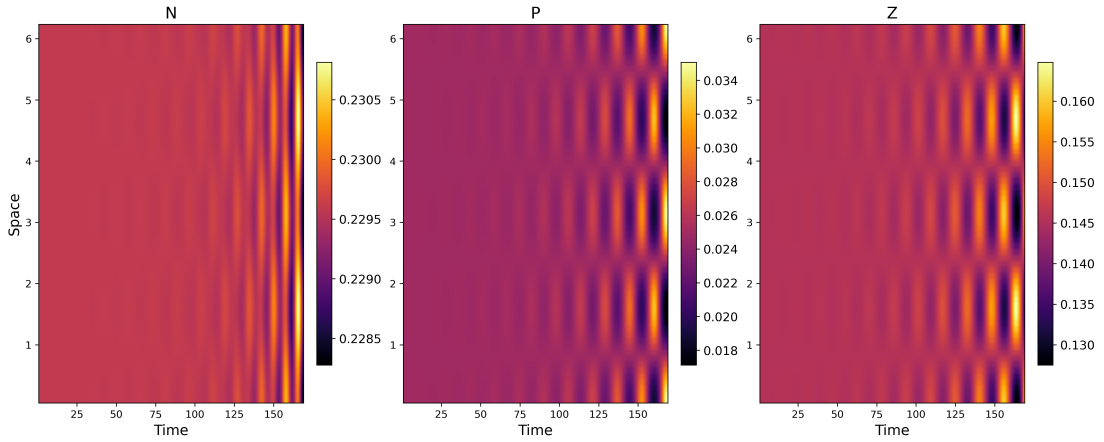


Figure 4.10: Evolution of NPZ model after initial perturbation with $k = 2$ mode.

As a simple check of our numerical method, we estimate the linear growth rate for this simulation. To do this we fit a line to the norm of the difference between each species and the corresponding equilibrium point. See Figure A.7. For each species, this fitted linear growth rate matched the real part of the eigenvalue to two decimal places. Moreover, We use the Fourier decomposition for the experimental perturbation and we can see that there is only one mode $k = 2$ showing in Figure A.8.

Random initial condition

Next we consider simulations with initial conditions that will excite all the unstable modes. We consider initial conditions in the form (4.4) with $W_j(x)$ generated randomly. See the following definition of each perturbation W_j:

$$W_j(x) = \epsilon_j(x), \quad \epsilon_j(x) \sim \mathcal{N}(0, \sigma^2) \tag{4.6}$$

where ϵ_j is a random variable which follows a normal distribution with standard deviation σ. We choose $\sigma = 10^{-5}$ in all the simulations for NPZ model.

We tested several values of the parameter d_1. For values of d_1 corresponding to the blue region in Figure 4.7, the solution decays back to the steady state. An example with $d_1 = 0.1$ is shown in Figure A.9.

Using a random initial condition, a combination of different modes is initially expected, and only the excited modes should grow and induce instabilities based on Figure 4.8. We can see that the spatial perturbations evolve in time from Figure 4.11.

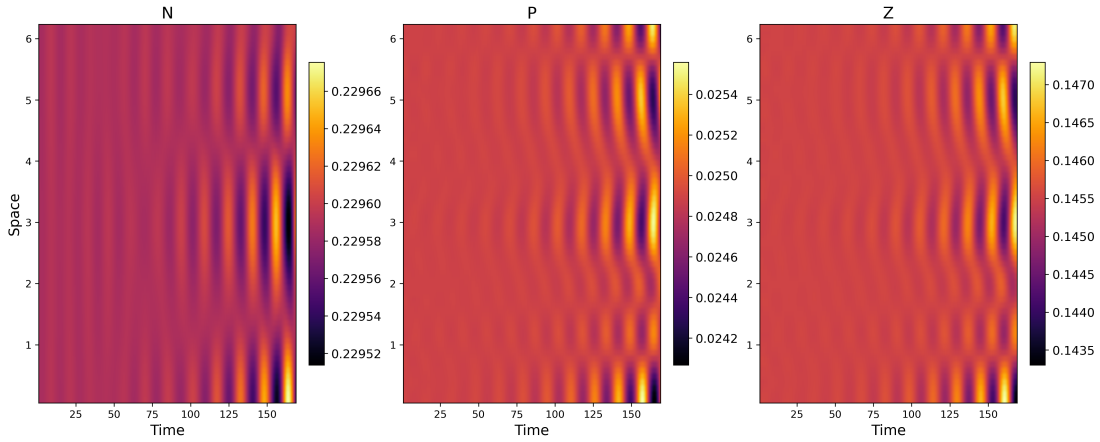


Figure 4.11: Evolution of NPZ model with random initial perturbation

To better understand diffusion induced instability from a random initial condition, we present the Fourier decomposition based on Figure 4.11. We can see the time emergence of each mode in Figure A.10. Decomposition of N contains modes with small wave number k from 1 to 2 and the decomposition of P and Z are similar containing wide range of modes from 1 to 4. We observe the emergence of unstable modes with $k > 4$ in Figure A.10, although these are less pronounced than the unstable modes from $k = 1$ to $k = 4$. This is consistent with Figure 4.8, which shows that the linear growth rate distribution over wave numbers is left-skewed toward lower k, so higher wave numbers correspond to smaller growth rates.

Furthermore, we run the simulation for a longer time in Figure 4.12 where the time ranges from 800 to 900 units of time. We see the amplitude of growing perturbation almost keeps constant compared to the clear linear growth in Figure 4.11.

4.4 NPZD Model

Recall from the previous section 3.3 that the conservation law introduces the total biomass as the total biomass, N_T, as a parameter in the equations for the equilibrium point of the ODE model. The value of N_T therefore affects the stability of the equilibrium point.

To study this, we fixed the rest of the model parameter as in Table 4.3, and chose a range of values for the total biomass N_T. We numerically solved the equilibrium equation (3.27) at each value of N_T and calculated the eigenvalues of the Jacobian of

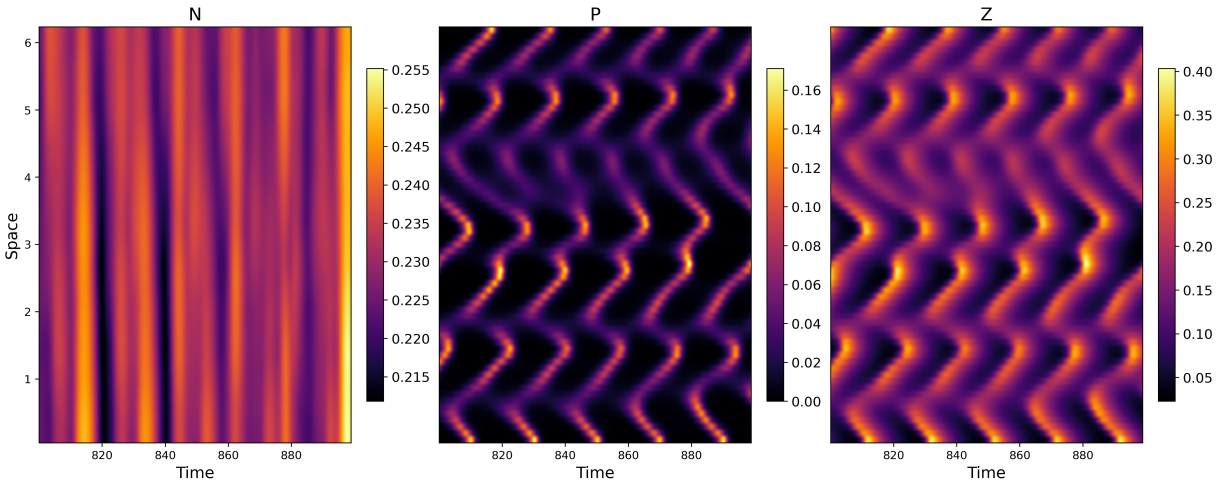


Figure 4.12: Longer Time Evolution of NPZ model after random initial perturbation

linearization (3.28). Figure 4.13 shows a plot of the largest real part of the eigenvalues, i.e. the linear growth rate, for each N_T. Note that since there is always one zero eigenvalue, the largest real part is always nonnegative.

4.4.1 Stability Without Diffusion

We can see in Figure 4.13 that an eigenvalue with positive real part emerges when $N_T \approx 0.5$. To study Turing instability we can take $N_T < 0.5$. Furthermore, based on Figure 4.14, larger total biomass N_T corresponds to the larger linear growth rate of PDE system. We thus choose $N_T = 0.4$ as the value for our numerical simulations. With this value, the equilibrium point is

$$[N^*, P^*, Z^*, D^*]^T \approx [0.2132,\ 0.0249,\ 0.1361,\ 0.0258]^T.$$

4.4.2 Diffusion Induced Instability

Recall the conditions in equation (3.35) for the Turing instability to potentially occur. To further study the possibility of Turing instability, we fixed all the reaction parameters as in Table 4.3 and chose $d_2 = d_4 = 0.0001 \ll d_3 = 0.001$. We then studied the Jacobian PDE J^*_{pde} eigenvalues from $k = 0.5$ to 9 and for a range of values of the nutrient

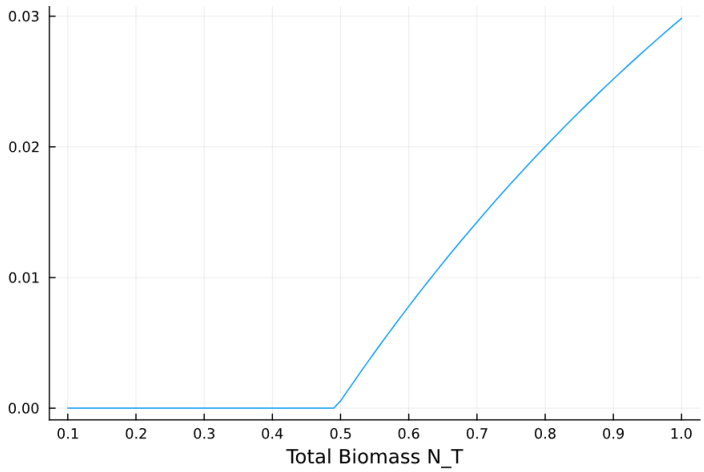


Figure 4.13: Dependence of linear growth rate of the ODE system (2.2) on the total biomass, N_T. Other parameter values are given in Table 4.3.

diffusion constant, d_1, and the total biomass, N_T. The results for $k = 1, 3, 7, 9$ are shown in Figure 4.14.

Recall from Figure 4.13, choosing the total biomass $N_T < 0.5$ ensures stability of the equilibrium point of the ODE model. For all the values of k we considered, stability persists in the PDE Jacobian for $N_T < 0.5$ and d_1 sufficiently small. Furthermore, we observed that with $N_T < 0.5$ and d_1 sufficiently large the Jacobian PDE has an eigenvalue with positive real part for all values of k except $k = 9$. Thus, the Turing instability is possible and may involve a variety of different modes. To further study the emergence of the Turing instability, we fix $N_T = 0.4$ and studied the maximum eigenvalue as a function of d_1 for the modes $0.5 - 9$. Figure 4.14 also qualitatively validates the condition (3.35) for the emergence of Turing instability.

Moreover, the analysis at the end of section 3.3 validates that the Turing instability can be seen for a certain set of wavenumber k and is possible to fail when k is large. Figure 4.14 shows that the blue region grows when k increases from $k = 3$ to $k = 9$ which predicts the analysis proceeding in section 3.3.

In section 3.3, we showed that $0 < m \leq 1$ ensured that certain terms in the Jacobian were negative as required for the possibility of Turing instability. We chose $m = 0.5$ so that these terms were clearly negative. As this is not a typical value of this parameter for plankton models, we explored the effect of this parameter on the eigenvalues of the PDE Jacobian p^*_{pde}, when $d_1 = 1$. Figure 4.15 shows the results. From this figure it is clear that decreasing m has a destabilizing effect as in the previous NP and NPZ models.

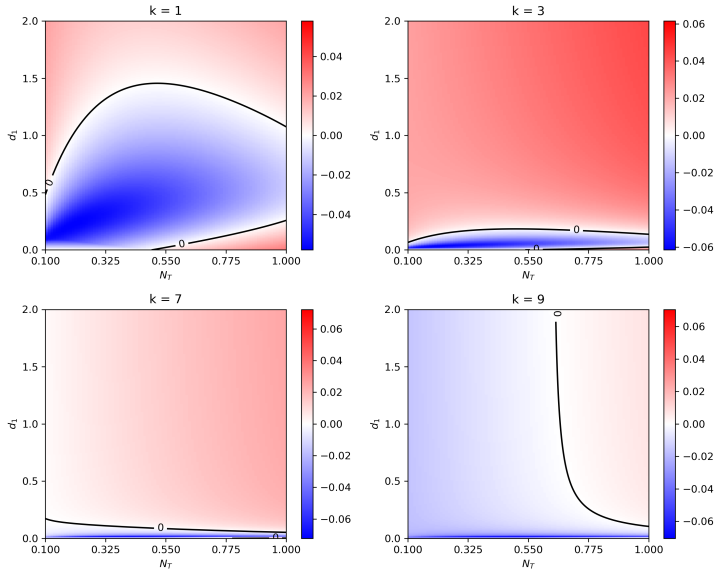


Figure 4.14: Dependence of linear growth rate of PDE model (2.9) on total biomass N_T and nutrient diffusion rate d_1 for modes k as shown. Other parameters values are given in Table 4.3

In summary, our linear stability analysis predicts that Turing instability will occur in the model (2.9) with the parameters given in Table 4.3 when the phytoplankton diffusion constant is increased from a small value to a large one. We will verify this predictions through numerical simulations of the full model in the next section.

4.4.3 Nonlinear simulations

In this section, results of simulations of the full nonlinear model (2.9) are presented. We will show that Turing instability does occur and verify that the linear growth rate in the simulations is as predicted by the linear stability analysis. The initial conditions are set up as perturbations from the equilibrium point:

$$[N,P,Z,D](x,0) = [N^*,P^*,Z^*,D^*] + [W_1,W_2,W_3,W_4](x),\ x \in [0,2\pi]. \tag{4.7}$$

We consider two choices for the perturbation functions: a single mode $\cos(3x)$ and random. The former is used to verify the linear growth of a single mode. The latter is to show the emergence of instability by a combination of various modes.

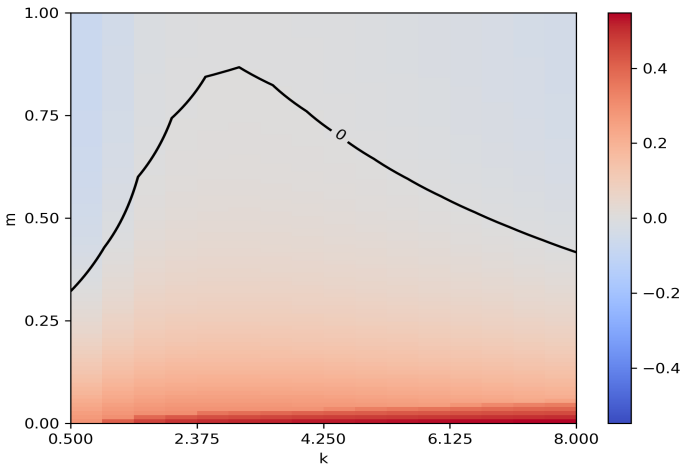


Figure 4.15: Dependence of linear growth rate of PDE model (2.9) on wave number k and phytoplankton mortality power m. Other parameters are given in Table 4.3.

Mode k=3

Figure 4.16 shows that for the parameters we consider, the largest linear growth rate of the PDE system corresponds to the mode $k = 3$. Thus, we take the initial perturbation function in the form

$$W_j(x) = c\cos(3\pi)\, v_{3j}, \tag{4.8}$$

where v_3 is the eigenvector associated with the eigenvalue with a positive real part for $k = 3$ and c is a scaling factor to control the magnitude of initial perturbation compared to the magnitude of equilibrium $[N^*, P^*, Z^*, D^*]$.

Figure 4.17 shows the simulation using the values of $d_1 = 1$ in the red region of the $k = 3$ plot in Figure 4.1, the solution grows. Note that the $k = 3$ mode structure of the solution is clearly visible at the end of the simulation. For values corresponding to the blue region of the $k = 3$ plot in Figure 4.14, the solution decays back to the steady state. An example can be found in Figure A.14 when $d_1 = 0.1$.

As a simple check of our numerical method, we estimate the linear growth rate for this simulation. To do this, we fit a line to the norm of the difference between the simulation results for each species and the corresponding equilibrium point. See Figure A.11. For each species, this fitted linear growth rate matched the real part of the eigenvalue to two decimal places.

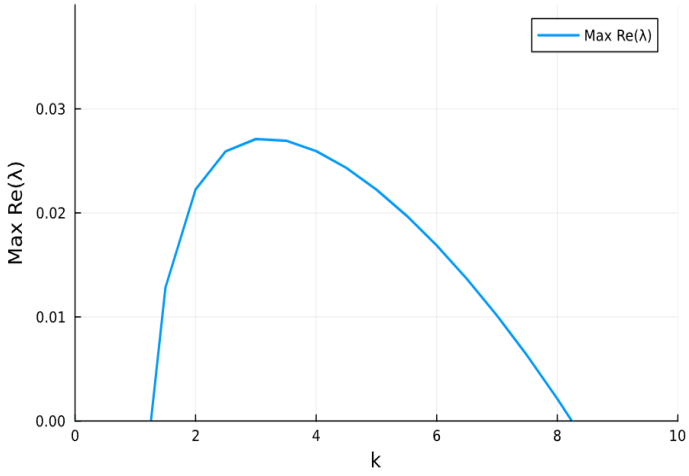


Figure 4.16: Dependence of linear growth rate of PDE model (2.9) on wave number k with $m = 0.5$. Other parameter are given in Table 4.3.

Random initial condition

Next, we consider simulations with initial conditions that will excite all the unstable modes. We consider initial conditions in the form (4.7) with $W_j(x)$ randomly generated. See the following definition of each perturbation W_j:

$$W_j(x) = \epsilon_j(x), \quad \epsilon_j(x) \sim \mathcal{N}(0, \sigma^2) \tag{4.9}$$

where ϵ_j is a random variable which follows a normal distribution with standard deviation σ. We choose $\sigma = 10^{-6}$ in all the simulations for NPZ model.

We tested several values of the parameter d_1. For values of d_1 corresponding to the blue region in Figure 4.14, the solution decays back to the steady state. An example with $d_1 = 0.05$ is shown in Figure A.12 indicating that $d_1 = 0.05$ is small enough to have no excited modes for a random initial condition.

Using a random initial condition, a combination of different modes is initially expected, and only the excited modes should grow and induce instabilities based on Figure 4.16. We can see that the spatial perturbations evolve in time from Figure 4.18.

To better understand diffusion induced instability from a random initial condition, we present the Fourier decomposition based on Figure 4.18. We can see the time emergence of each mode in Figure A.13. The decomposition of N contains modes with a wide range of wave numbers k from 1 to 5 and the decomposition of P, Z and D are similar containing a small range of modes from 3 to 5.

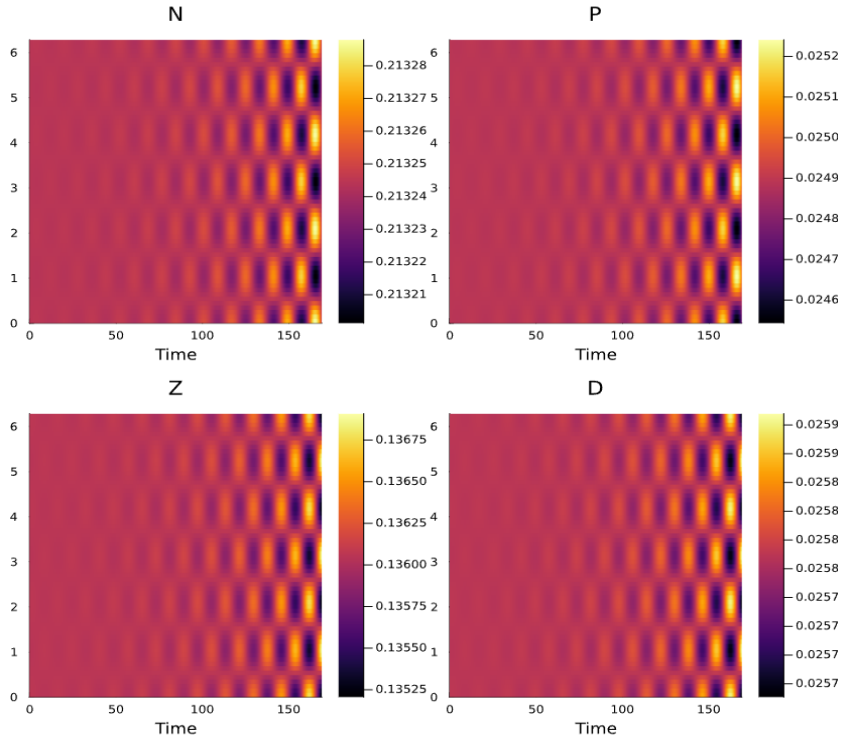


Figure 4.17: Evolution of NPZD model after initial perturbation with $k = 3$ mode

Furthermore, we run the simulation for a longer time in Figure 4.19 where the time ranges from 800 to 900 units of time. We see the amplitude of the perturbation almost remains constant compared to the clear linear growth in Figure 4.18.

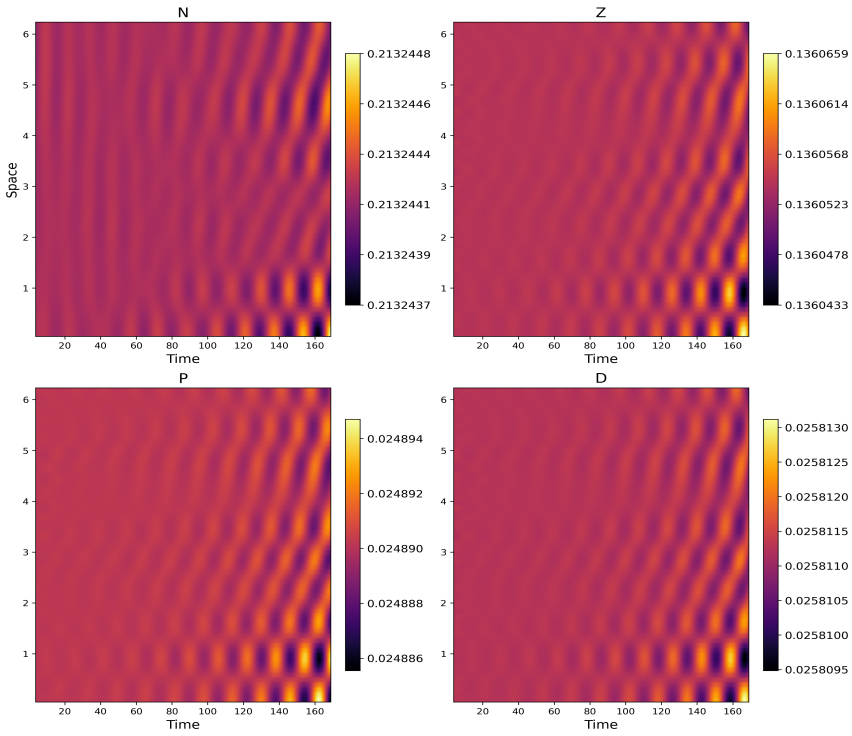


Figure 4.18: Evolution of NPZD model with random initial perturbation

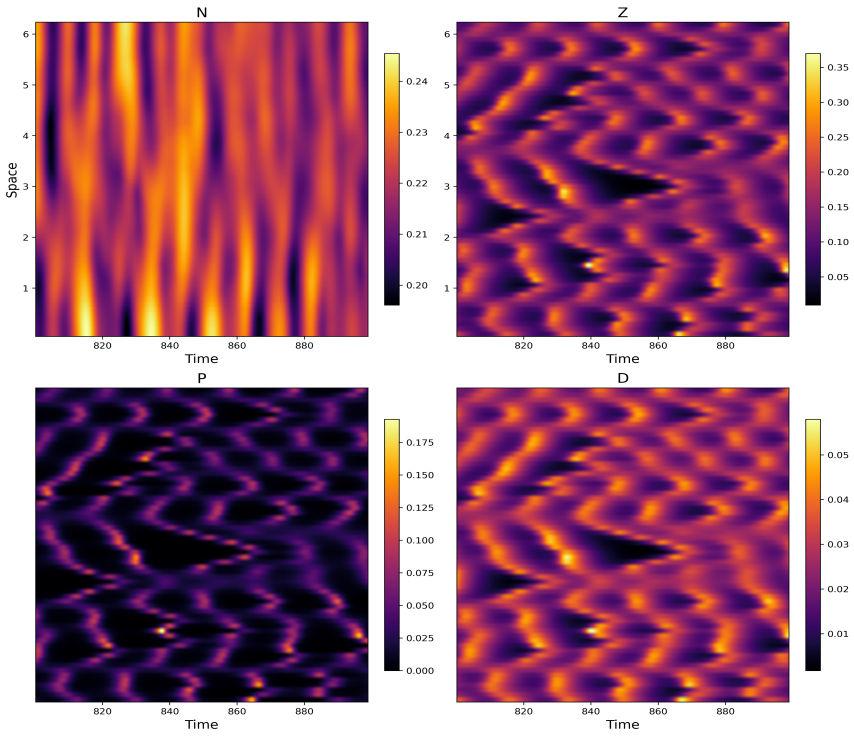


Figure 4.19: Longer Time Evolution of NPZD model after random initial perturbation

Chapter 5

Conclusion

In this research, our core contribution is that we discover and validate the impact of different scales of diffusion coefficients on Turing instability in conservative plankton models. We begin by introducing the concept of Turing instability and proposing a specific form of perturbation given by (3.4).Assuming the perturbation form, we analyze the model parameters to examine the potential for Turing instability in Section 3. Specifically, we investigate sign changes in the constant coefficient b_0 of the characteristic polynomial across all models to assess the conditions under which Turing instability may arise, focusing on the relative magnitudes of the diffusion coefficients. We also study the influence of parameter m on Turing instability. A typical choice of $m = 1$ in plankton modeling can be seen in [12] and [25]. Through this analysis, we identify that conditions (3.11), (3.20), (3.35), together with $0 < m < 1$, are critical for the onset of Turing instability. These conditions consistently require a substantial difference between d_1 and the other diffusion coefficients.

We use the results on parameters found in the model chapter to run the numerical simulations. Several results from numerical simulations are used to validate the Turing instability such as the linear growth rate.

We extend the research on the analysis of Turing instability from two compartmental model in [18] to three and four compartmental models. We show different diffusion coefficients induce Turing instability which is a extension work from [25] that equal diffusion coefficients enhance the stability. We obtained the verification of time evolution with the compatible linear growth rate of the spatially unstable modes. This is the main contribution we have in this research. Our research shows that the Turing instability is closely related to the scales of diffusion coefficients of different species. Turing instability can occur not only in the two species reaction diffusion model but also in three and four species reaction diffusion models. Our analysis shows the characteristic polyno-

mial coefficient b_0 is likely to break the stability criterion relative to other coefficients. Figures 4.5, 4.8, and 4.18 illustrate that nutrients tend to exhibit excited modes with lower wavenumbers k compared to other species under random initial conditions. In all numerical simulations, the diffusion coefficient d_1 for nutrients is the largest among all species, leading to a stronger smoothing effect on spatial variations, particularly at higher frequencies.

In addition, there are many more future directions for research. For example, we only study the one-dimensional model here in depth z, but it is worth studying the models in a higher dimensional space. More importantly, we apply only one methodology to break the stability criterion using Routh array method that $b_0 < 0$. We show that the mortality power of phytoplankton $0 < m \leq 1$ is very important for Turing instability and smaller m destabilizes the system numerically. However, $b_0 < 0$ is one of the sufficient conditions, there could be other sufficient conditions to explore in future work. In this thesis, only one fixed format of reaction in the model is studied, which can enrich the reaction term to build a more realistic model. For example, there could be some waste amount that contributes to the detritus when zooplankton eats phytoplankton.

References

[1] Chelsie E Armbruster and Harry LT Mobley. Merging mythology and morphology: the multifaceted lifestyle of proteus mirabilis. *Nature Reviews Microbiology*, 10(11):743–754, 2012.

[2] Edoardo Beretta, GI Bischi, and Fortunata Solimano. Stability in chemostat equations with delayed nutrient recycling. *Journal of Mathematical Biology*, 28(1):99–111, 1990.

[3] Olivier Bernard, Annie Sciandra, et al. A 2D model for hydrodynamics and biology coupling applied to algae growth simulations. *ESAIM: Mathematical Modelling and Numerical Analysis*, 47(5):1515–1535, 2013.

[4] Jeff Bezanson, Alan Edelman, Stefan Karpinski, and Viral B Shah. Julia: A fresh approach to numerical computing. *SIAM Review*, 59(1):65–98, 2017.

[5] Navid C. Constantinou, Ali Ramadhan, Gregory LeClaire Wagner, James R. Adkins, Valentin Churavy, Gael Forget, Baptiste Foures, Andrey F. Pletzer, Andrea Piantadosi, and William R. Young. Oceananigans.jl: Fast and friendly geophysical fluid dynamics on cpus and gpus, April 2020.

[6] Richard Courant, Kurt Friedrichs, and Hans Lewy. On the partial difference equations of mathematical physics. *IBM Journal of Research and Development*, 11(2):215–234, 1967.

[7] Yihong Du and Linfeng Mei. On a nonlocal reaction–diffusion–advection equation modelling phytoplankton dynamics. *Nonlinearity*, 24(1):319, 2010.

[8] Peter JS Franks. NPZ models of plankton dynamics: their construction, coupling to physics, and application. *Journal of Oceanography*, 58(2):379–387, 2002.

[9] Peter JS Franks, Joe S Wroblewski, and Glenn R Flierl. Prediction of phytoplankton growth in response to the frictional decay of a warm-core ring. *Journal of Geophysical Research: Oceans*, 91(C6):7603–7610, 1986.

[10] Wendy Gentleman. A chronology of plankton dynamics in silico: how computer models have been used to study marine ecosystems. *Hydrobiologia*, 480(1):69–85, 2002.

[11] Xue-Zhong He and Shigui Ruan. Global stability in chemostat-type plankton models with delayed nutrient recycling. *Journal of mathematical biology*, 37(3):253–271, 1998.

[12] Matthew Kloosterman, Sue Ann Campbell, and Francis J Poulin. A closed NPZ model with delayed nutrient recycling. *Journal of mathematical biology*, 68(4):815–850, 2014.

[13] Tibor Kmet'. Material recycling in a closed aquatic ecosystem. I. Nitrogen transformation cycle and preferential utilization of ammonium to nitrate by phytoplankton as an optimal control problem. *Bulletin of mathematical biology*, 58(5):957–982, 1996.

[14] Andrew L Krause, Václav Klika, Philip K Maini, Denis Headon, and Eamonn A Gaffney. Isolating patterns in open reaction–diffusion systems. *Bulletin of Mathematical Biology*, 83(7):82, 2021.

[15] Yunxiang Lu, Min Xiao, Gong Chen, Binbin Tao, Shi Chen, and Jiaxuan Liu. Turing instability analysis of marine planktonic ecosystem under the influence of spatial heterogeneity. In *2021 33rd Chinese Control and Decision Conference (CCDC)*, pages 5333–5338. IEEE, 2021.

[16] Anna Marciniak-Czochra, Grzegorz Karch, and Kanako Suzuki. Instability of turing patterns in reaction-diffusion-ODE systems. *Journal of mathematical biology*, 74(3):583–618, 2017.

[17] Pierre Marrec, Gérald Grégori, Andrea M. Doglioli, Mathilde Dugenne, Sandra Nunige, and et al. Coupling physics and biogeochemistry thanks to high-resolution observations of the phytoplankton community structure in the northwestern mediterranean sea. *Biogeosciences*, 15(5):1579–1606, 2018.

[18] James D Murray. *Mathematical biology: I. An introduction*, volume 17. Springer Science & Business Media, 2007.

[19] Katsuhiko Ogata. *Modern control engineering*. Prentice hall, 2010.

[20] RA Parker. Eddy diffusion of phytoplankton and nutrients: estimating coefficients from simulated and observed vertical distributions. *Journal of plankton research*, 13(4):815–830, 1991.

[21] Francis J Poulin and Peter JS Franks. Size-structured planktonic ecosystems: constraints, controls and assembly instructions. *Journal of plankton research*, 32(8):1121–1130, 2010.

[22] Jennifer C Prairie, Kelly R Sutherland, Kerry J Nickols, and Amanda M Kaltenberg. Biophysical interactions in the plankton: A cross-scale review. *Limnology and Oceanography: Fluids and Environments*, 2(1):121–145, 2012.

[23] Yangyang Shao, Yan Meng, and Xinyue Xu. Turing instability and spatiotemporal pattern formation induced by nonlinear reaction cross-diffusion in a predator–prey system with allee effect. *Mathematics*, 10(9):1500, 2022.

[24] Hal L Smith and Paul Waltman. *The theory of the chemostat: dynamics of microbial competition*, volume 13. Cambridge University Press, 1995.

[25] Yiwen Tao, Sue Ann Campbell, and Francis J Poulin. Dynamics of a diffusive nutrient-phytoplankton-zooplankton model with spatio-temporal delay. *SIAM Journal on Applied Mathematics*, 81(6):2405–2432, 2021.

[26] Vinicius Beltram Tergolina, Enrico Calzavarini, Gilmar Mompean, and Stefano Berti. Effects of large-scale advection and small-scale turbulent diffusion on vertical phytoplankton dynamics. *Physical Review E*, 104(6):065106, 2021.

[27] Alan Mathison Turing. The chemical basis of morphogenesis. *Bulletin of mathematical biology*, 52(1):153–197, 1990.

[28] Robert A Van Gorder. Pattern formation from spatially heterogeneous reaction–diffusion systems. *Philosophical Transactions of the Royal Society A*, 379(2213):20210001, 2021.

[29] Edgardo Villar-Sepúlveda and Alan R Champneys. General conditions for Turing and wave instabilities in reaction-diffusion systems. *Journal of Mathematical Biology*, 86(3):39, 2023.

[30] Edgardo Villar-Sepúlveda, Alan R Champneys, and Andrew L Krause. Designing reaction-cross-diffusion systems with Turing and wave instabilities: E. villar-sepúlveda et al. *Journal of Mathematical Biology*, 91(4):37, 2025.

APPENDICES

Appendix A

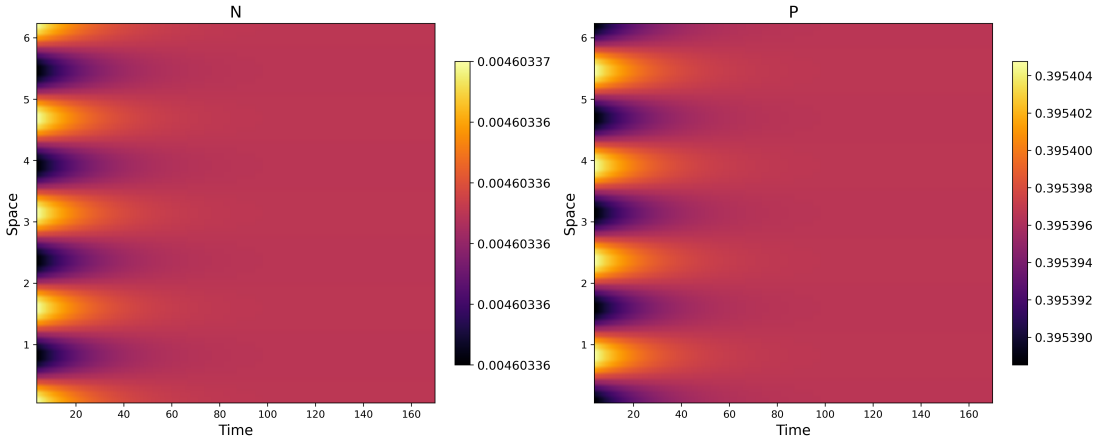


Figure A.1: Evolution of NP model after initial perturbation with $k = 4$ and $d_2 = 0.004$. Other parameter values are given in Table 4.1.

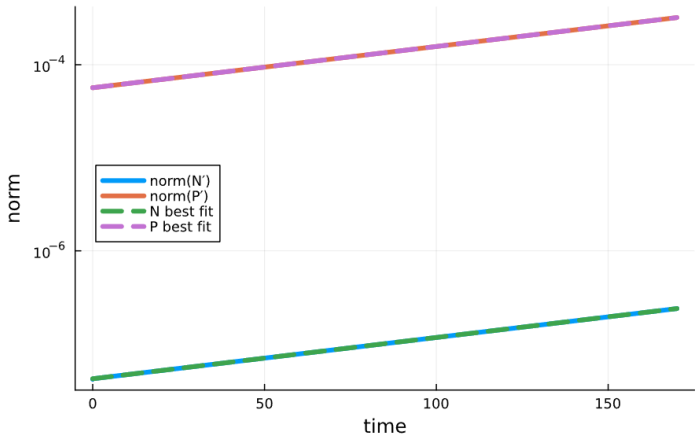


Figure A.2: Linear fit of logarithm growth of simulation in Figure 4.4

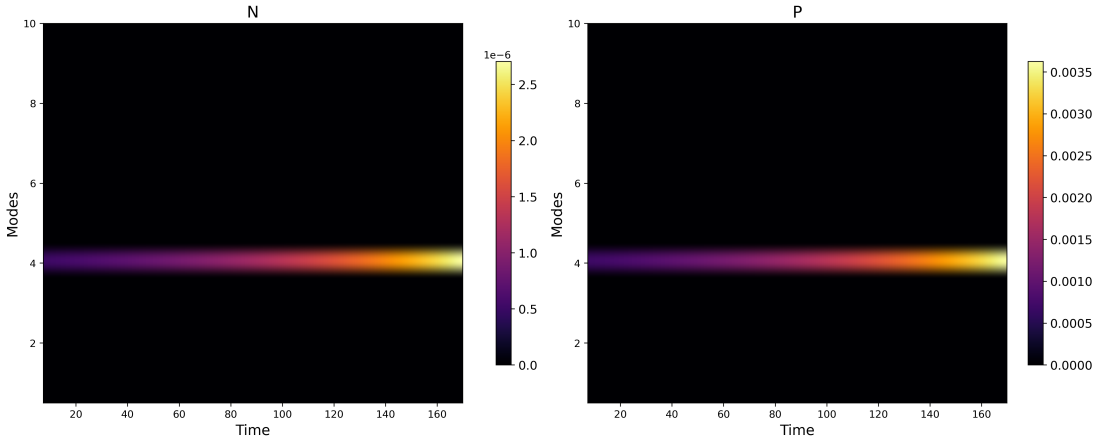


Figure A.3: Power spectrum from Fourier decomposition of simulation in Figure 4.4

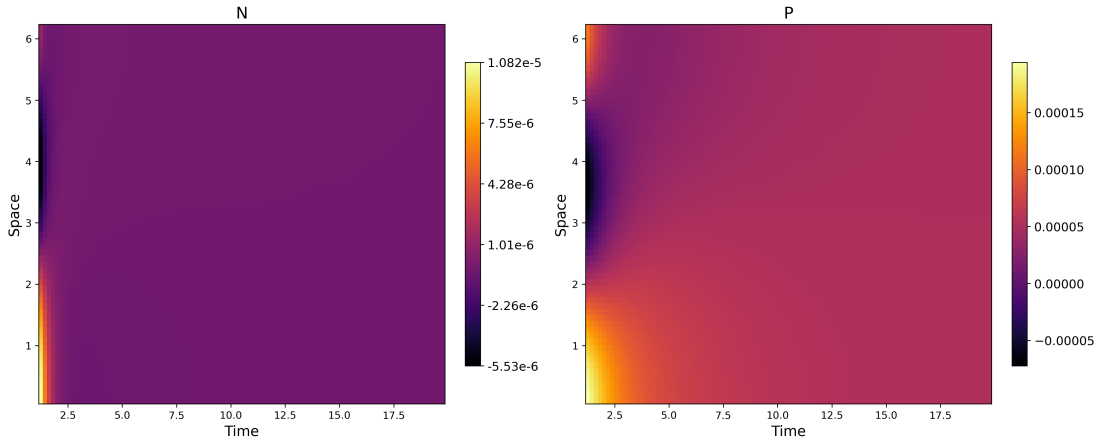


Figure A.4: Evolution of NP model after random initial perturbation with $d_2 = 1$. Other parameter values are given in Table 4.1.

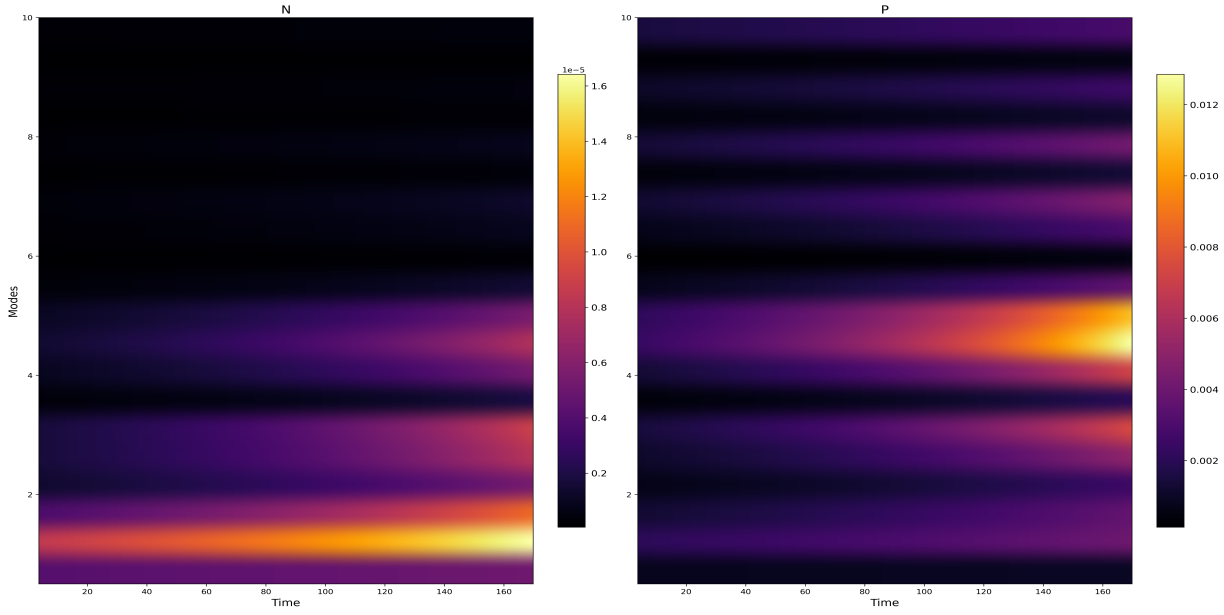


Figure A.5: Power spectrum from Fourier decomposition of simulation in Figure 4.5

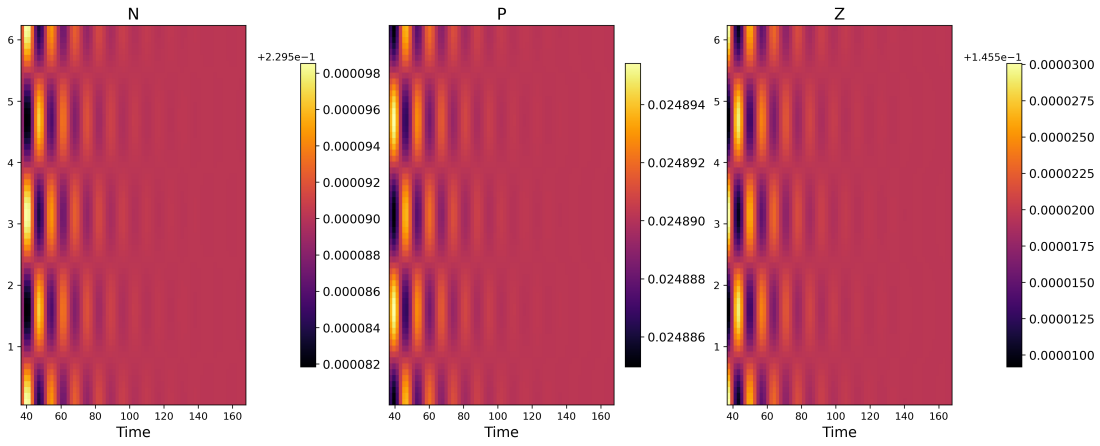


Figure A.6: Evolution of NPZ model after initial perturbation with $k = 2$ and $d_1 = 0.1$. Other parameter values are given in Table 4.2.

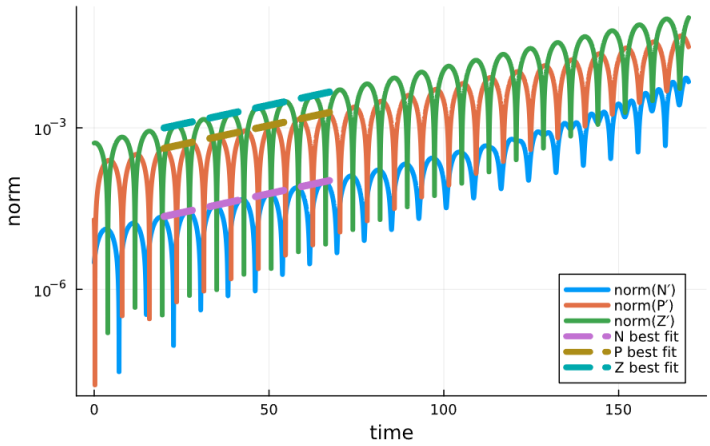


Figure A.7: Linear fit of logarithm growth of simulation in Figure 4.10

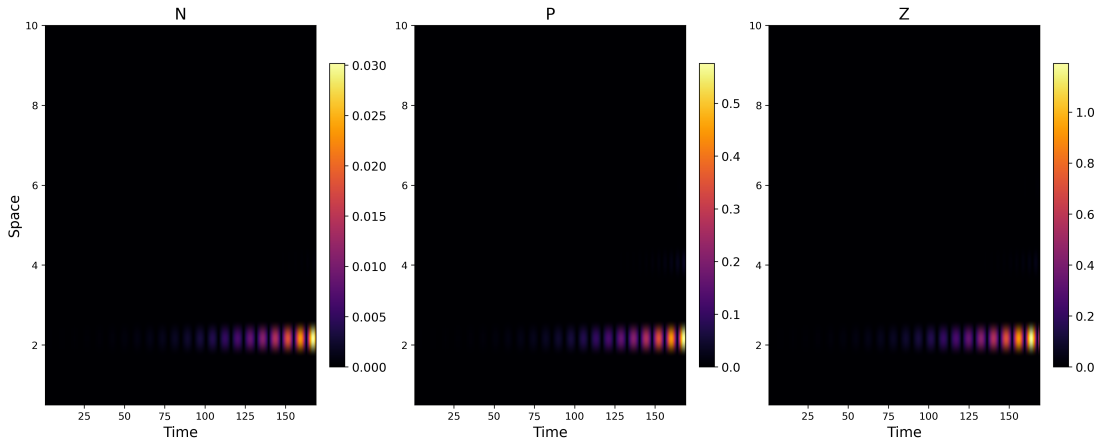


Figure A.8: Power spectrum from Fourier decomposition of simulation in Figure 4.10

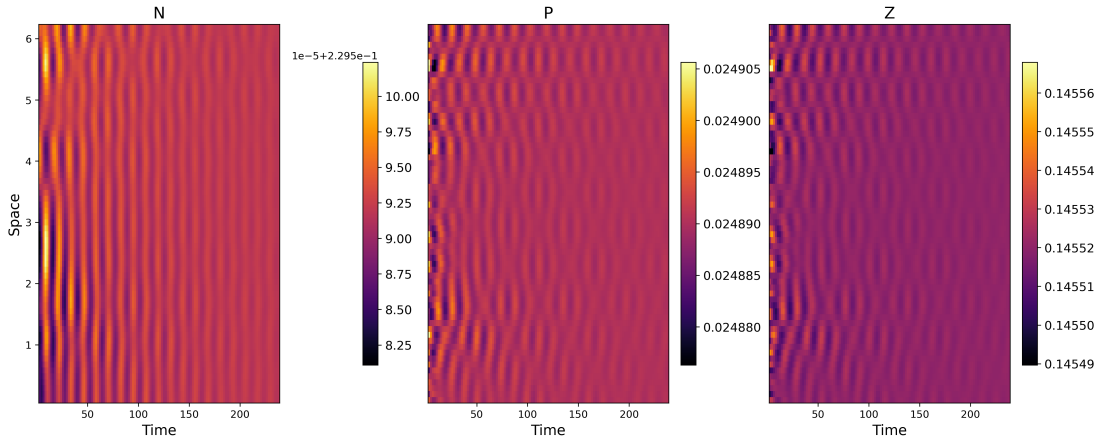


Figure A.9: Evolution of NP model after random initial perturbation with $d_1 = 0.1$. Other parameter values are given in Table 4.2.

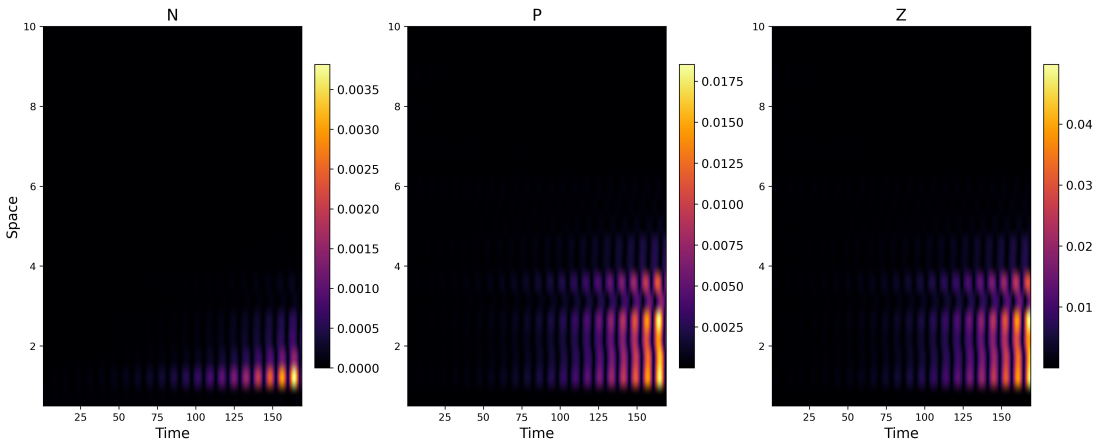


Figure A.10: Power spectrum from Fourier decomposition of simulation in Figure 4.11

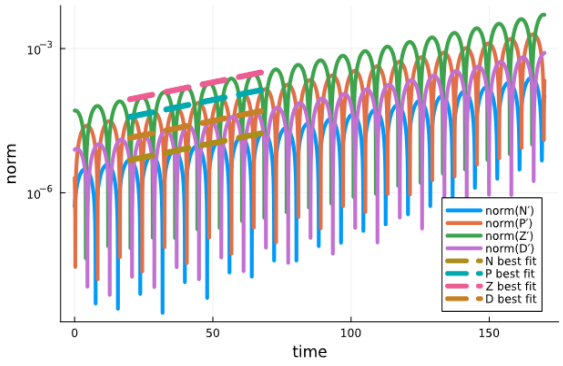


Figure A.11: Linear fit of logarithm growth of simulation in Figure 4.17

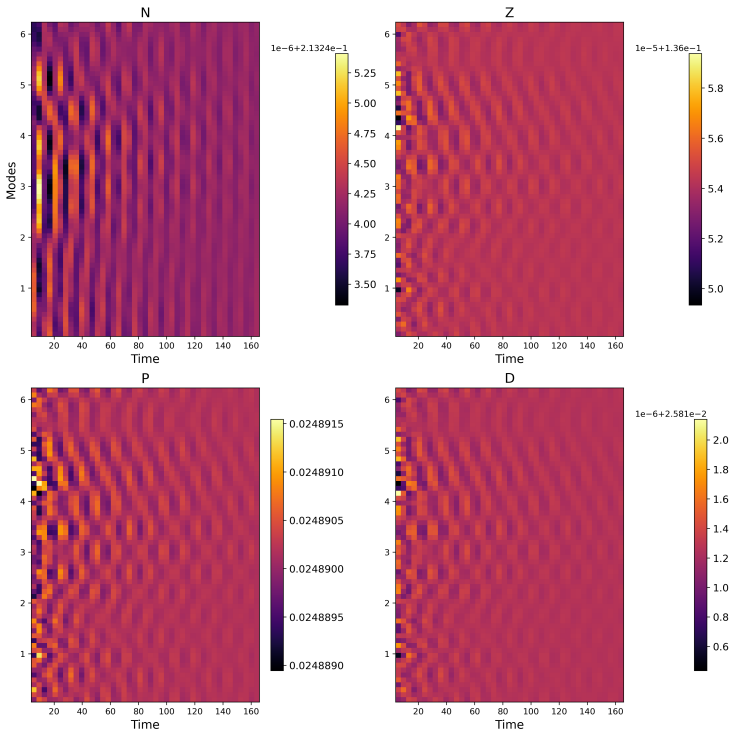


Figure A.12: Evolution of NPZD model after random initial perturbation with $d_1 = 0.05$. Other parameter values are given in Table 4.3.

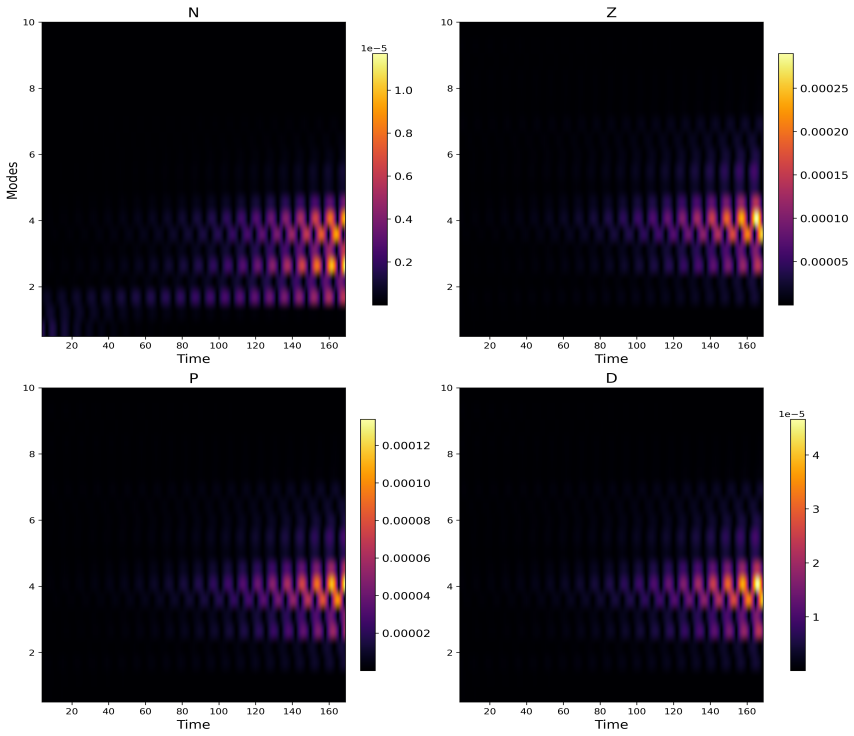


Figure A.13: Power spectrum from Fourier decomposition of simulation in Figure 4.18

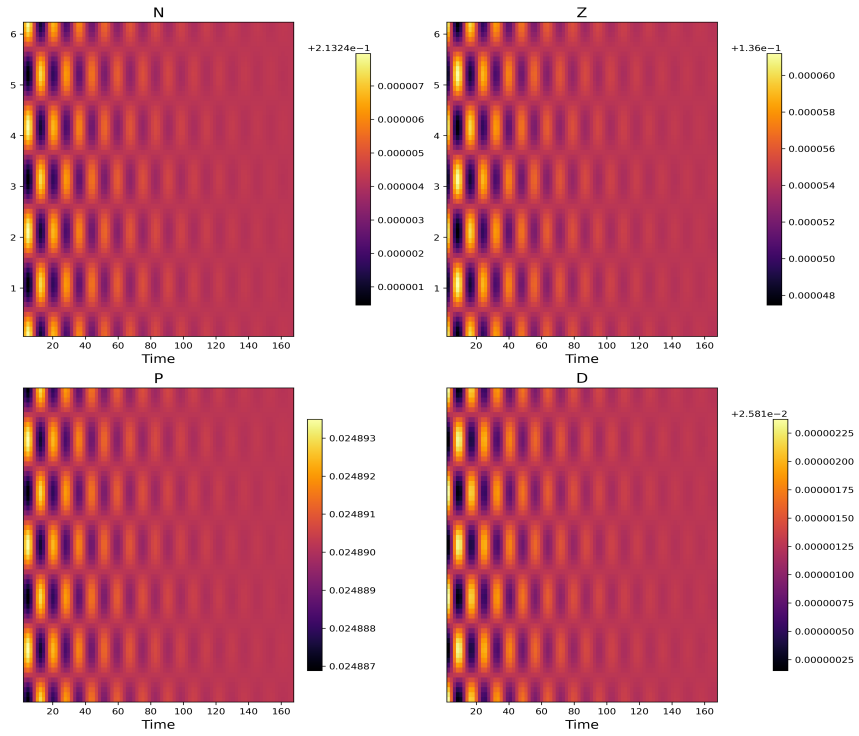


Figure A.14: Evolution of NPZD model after initial perturbation with $k = 3$ and $d_1 = 0.1$. Other parameter values are given in Table 4.3.